AALBORG UNIVERSITY
DENMARK

Andreas Richard Lichtenberg

System design and trial of combined photovoltaics and membrane distillation

AALBORG UNIVERSITY
DENMARK

Department of Chemistry and Bioscience
Fredrik Bajers Vej 7H
DK-9220 Aalborg Ø
http://en.bio.aau.dk

Title:
System design and trial of combined photovoltaics and membrane distillation

Theme:
Engineering / desalination / waste heat utilization

Project Period:
fall 2021 and spring 2022

Participant(s):
Andreas Richard Lichtenberg

Supervisor(s):
Donghong Yu
Aamer Ali

Page Numbers: 52

Date of Completion:
June 9, 2022

Abstract:

A combined process of photovoltaics and membrane distillation was tested in a controlled environment to investigate cooling effect on open circuit voltage of a small solarpanel, a parameter directly correlated to power output in normal temperature ranges. It was consistently shown that the combined system successfully utilized waste heat energy to power the membrane distillation, but power output was reduced in some experiments. Furthermore, the lack of a mechanism of heat transfer from the combined module, lead to a further build-up of heat, lowering flux compared to expectation. A flow cooling system was also tested, wherein salted water would pass behind the panel and slowly drip to a beaker at different flow rates. It was found that high flow rate had a positive impact on temperature.

Preface

This work is a master thesis from the Department of Chemistry and Bioscience at Aalborg University. The topic is separation chemistry, and the primary focus is delivering heat to a membrane distillation system by combining the system with a solar panel

Special thanks to supervisors Donghong Yu and Aamer Ali for council and good discussions, and to fellow student Morten Haugaard Nielsen for supplying ceramic membranes for a part of the work. Thanks to follow student Gustav Simoni and technical assistant Jan Christiansen at the department of Energy for expertise and equipment for 3D printing. Thanks to Tamas Kerekes in AAU's department of Energy, for helping both with supplying the solar panel and characterizing it. A personal thanks to David Godiksen, Barbara Ballarini, Steffen Lykke Christensen, Lærke Nørgaard Madsen, Sara Muñana and Morten Haugaard Nielsen, with whom I shared an office during the work, for continued helpful discussions and mutual support.

Aalborg University, June 9, 2022

Andreas Richard Lichtenberg
<alicht17@student.aau.dk>

	Abbreviation	Description
ABS	Acrylonitrile butadiene styrene	
AGMD	Air Gap Membrane Distillation	
ASA	Acrylonitrile styrene acrylate	
CB	Conduction Band	
DI water	deionized water	
DCMD	Direct Contact Membrane Distillation	
eV	Electron Volts	
EDI	Energy Displacement Index	
FF	Fill factor	
F-POSS	Fluorinated Polyhedral Oligomeric Silsesquioxane	
GERD	Grand Ethiopian Renaissance Dam	
I_{rr}	irradiance	
LEP	Liquid entry pressure	
LMH	Liters per square meter per hour	
MD	Membrane Distillation	
V_{oc}	Open Circuit Voltage	
PV	Photovoltaics	
PTFE	Polytetrafluoroethylene	
PCE	Power Conversion Efficiency	
RO	Reverse Osmosis	
I_{sc}	short circuit current	
Si-C	Silicon Carbide	
SGMD	Sweep Gas Membrane Distillation	
VB	Valence Band	
VMD	Vacuum Membrane Distillation	

Table of content

1 Introduction

Throughout history, Egypt and its predecessors have been dependent on the Nile as the main artery. This remains true to this day, as in 2007, all of Egypts fresh water came from the Nile alone.[1] Despite this, the Egyptians have never owned the springs of the Nile. Lake Tana, also referred to as the Blue Nile, contributes most of the water to the Nile, and has its springs in the Ethiopian highlands.[2] Coincidentally, the Ethiopian government is building a dam from this river basin, known as the Grand Ethiopian Renaissance Dam project (GERD). The aim of GERD is to retain more water from the springs, and create wealth and stability from the immense amounts of hydropower GERD could produce, as well as retaining the water for longer to better irrigate the soil. Initially, this project greatly concerned the Egyptians, who worried the project would dry up the Nile.[3] While this issue has been mostly resolved now, by compromises by both governments, this conflict greatly demonstrates the needs in modern society for water and electricity.

As the world looks to eliminate the use of fossil fuel over the coming decades, the future options for producing electricity consist of a large variety of renewable methods, such as solar-, wind-, hydro-, or nuclear power. While hydro- and nuclear power have remained relatively stagnant in terms of efficiency, and advancements in wind power mostly rely on material science innovations to build larger turbines, photovoltaics (PV) have seen rampant improvements over the last decades. One issue that remains for solar technology is the side-production of heat during electricity production. This heat has thus far been considered waste, and the higher operating temperatures of the solar panel increases structural damage to the lattice, reducing the effective lifespan. [4, 5] Therefore, finding an effective way to employ this by-product heat would increase output and lifespan of the PV in addition to saving the cost of creating heat for other purposes.

Membrane distillation (MD) is a somewhat well known technology, originally dubbed as MD at the "workshop on Membrane Distillation" in Rome in 1986. [6] It is a thermally driven separation process, most commonly applied to distil water at temperatures far below the boiling point of 100°C at atmospheric pressure. The most pressing issue for this technology is the efficiency; when compared to other membrane separation processes such as reverse osmosis (RO), the cost pr. volume clean water is higher for MD. The obvious reason for this is the cost of heating the feed water, and thus finding a way to produce heat that comes at low or no cost is crucial when implementing MD. In recent years, there has been a staggering growth in the scientific interest in MD. Despite this, commercial investment and applications have remained somewhat low. The main reasons for this commercial disinterest have been the aforementioned high thermal energy cost and a lack of specifically designed modules or integrated systems. [7]

This work proposes and explores a combination of the two aforementioned technologies: a system in which the waste heat from PV electricity production can be used as the heat source for an MD system to produce ultra-pure water from brine or other waste streams.

2 Problem Analysis

2.1 Membrane distillation

As mentioned in chapter 1, MD is a thermal separation process. Fundamentally, it is operated under a thermal gradient as opposed to a hydraulic pressure gradient, like RO for example. The driving force of MD is a gradient in vapor pressure across a hydrophobic membrane. The hydrophobic membrane prevents the flow of liquid water from the heated feed to the cooled permeate, however gaseous water molecules may pass through the membrane due to its large pore size. This process takes place in both directions, however due to a gap in vapor pressure, net flux is observed from feed to permeate, and the rejection is effectively 100% for any non-volatile compounds polluting the feed. The value of this flux depends on temperature, as larger gaps in temperature would lead to faster transport. [8]

The practical setup may vary in complexity and efficiency; generally there are 4 main methods: Direct contact MD (DCMD), air gap MD (AGMD), sweep gas MD (SGMD), and vacuum MD (VMD). [8] VMD is likely to produce the largest flux, as the vapor pressure on the permeate side can reasonably be approximated as 0, maximizing the net produce. The drawback for VMD is the expense of the vacuum condition; as MD is often projected as a cheap alternative in areas where waste-heat is abundant, the requirement of a vacuum chamber on the permeate side presents a steep increase in net price. As such, the majority of research and applications all the way from lab- to commercial scale has been DCMD.

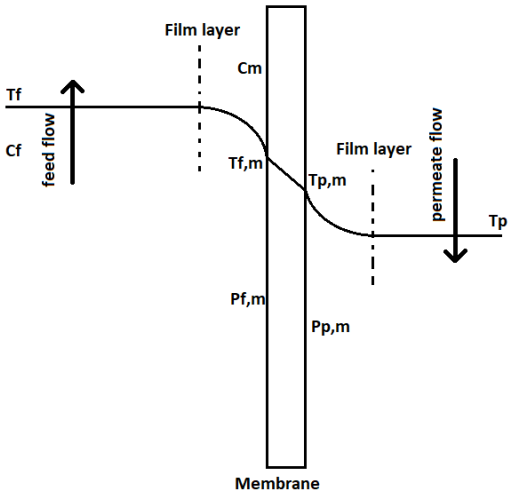

Figure 2.1. DCMD setup illustration[8]

2.2 Photovoltaics

The photoelectric effect is a physical- and chemical-principle in which light absorption can create an electrical current and voltage in a material. While the massive and promising industry of solar power is relatively new, the principle discovery of the photovoltaic effect is quite old, and can be traced all the way back to French natural Philosopher Edmund Becquerel, who, in 1839, did experiments with two metal electrodes in an aqueous solution. [9] This, in today's vocabulary, would be described as a Photoelectrochemical PV cell. While breakthroughs would continue to happen, first with the discovery of photoconductivity in Silicon by Willoughby Smith in 1873, the first photoelectric effect demonstration with naturally formed defect junctions in silicon was performed in 1941; over a century after the principle discovery. [9] Regardless of how marvellous these discoveries must have seemed at the time, the efficiencies of power conversion were extremely low by today's standards, and the power that was created was very costly, at about 1500$ pr. watt. [9]

In more recent times, power conversion efficiencies (PCE) have risen dramatically from the 2% sold by Western Electric and Hoffman Electronics in the 1950s, to about 20% in the 2010s. [9, 10] With so high PCEs, elimination of factors that multiplicatively reduce PCE is now much more significant than ever, and thus interest in the effects of external factors has spiked. Operating temperature in the cell has been shown to hamper PCE of PVs. [11, 12] As such, studies on the commercial feasibility of cooling PVs during operation have been conducted. More than 50% of the energy from solar radiation is turned into heat in the panel, increasing operating temperature from room temperature to around 60°C when the sunlight is strongest.[13] Teqwa et al. found an increase in the energy harvested with an automatic water cooling system that would wash the surface of the PV with water when a sensor detected a surface temperature greater than 36°C. [13] While such a strategy may increase power output slightly, it can be considered very wasteful of water.

3 Problem Statement

3.1 problem definition

With the operating conditions of MD and the thermal disadvantages of PV established in previous sections, the combination of the two technologies seems apt. It is worth investigating whether these technologies may have the solution to each other's problem.

MD can provide a clean and sustainable production of ultra-pure water that can then either be re-salted for potable purposes or used directly as desalinated water.

PV can provide clean and sustainable production of electricity at very competitive prices on the current market.

A large problem for PV is heat generated as a side product which not only reduces PCE outright, but also shortens the lifespan of the panel due to increased structural damage under prolonged operation at elevated temperatures. MD, meanwhile, cannot compete with other membrane separation technologies in terms of cost without a source of free or cheap low-grade thermal energy. Here is where the application of their combination should become apparent: A system in which by-product heat is taken from the PV and used in the feed solution of an MD plant.

Such work can mostly be regarded as an engineering puzzle of optimization: how much thermal energy can realistically be harvested from PV, and how does this harvest impact both the efficiency of the PV and the operating cost of MD. For this purpose, AGMD and VMD will be employed.

4 Theory

4.1 Membrane Distillation

As briefly mentioned in section 2.1, the driving force in MD is thermal and manifests as a result of the vapor pressure gradient over a hydrophobic membrane. The applications of this high-rejection separation process ranges from desalination of sea water to precipitation of precious salts or concentration of fruit juices. [8] When evaluating such a separation process, the mechanisms for transfer of both mass and heat are important, as a larger convection heat transfer over the membrane will make the process more expensive due to heat losses, and the mass transfer determines the rate of the process.

4.1.1 mass transfer

As the driving force for the mass transfer mechanism has been established as a gradient in vapor pressure, the equation to describe flux through the membrane can be described as follows:

$$J = C_m(P_f - P_p) \tag{4.1}$$

Where P_f and P_p are vapor pressures at the membrane surface of feed and permeate side respectively. C_m is the membrane coefficient which is unique for each type of membrane material. [8] The vapor pressures in equation 4.1 can be quite hard to measure experimentally, and as such it is often inferred due to its correlation with temperature, resulting in the following equation:

$$J = C_m \frac{dP}{dT}(T_f - T_p) \tag{4.2}$$

The conversion factor of vapor pressure to temperature varies depending on temperature, as described by $\frac{dP}{dT}$, and this can be given by the Clausius-Clapeyron equation:

$$\frac{dP}{dT} = [\frac{\Delta H_v}{RT^2}]P_0(T) \tag{4.3}$$

Where ΔH_{vap} is the heat enthalpy of vaporization, R is the gas constant and $P_0(T)$ is the saturated vapor pressure at a given temperature. Expanding this equation to finding a vapor pressure at a specific temperature yields:

$$ln(\frac{P_1}{P_2}) = -\frac{\Delta H_{vap}}{R}(\frac{1}{T_1} - \frac{1}{T_2}) \tag{4.4}$$

Using a known vapor pressure and temperature, for example the boiling point in atmospheric pressure, the vapor pressure at any given temperature may be calculated as:

$$P_x = 1 * e^{(-(\frac{\Delta H_{vap}}{R})(\frac{1}{T_x} - \frac{1}{T_{boil}})} \tag{4.5}$$

This function will essentially lead to the creation of the phase diagram. The water phase diagram is displayed below as an example:

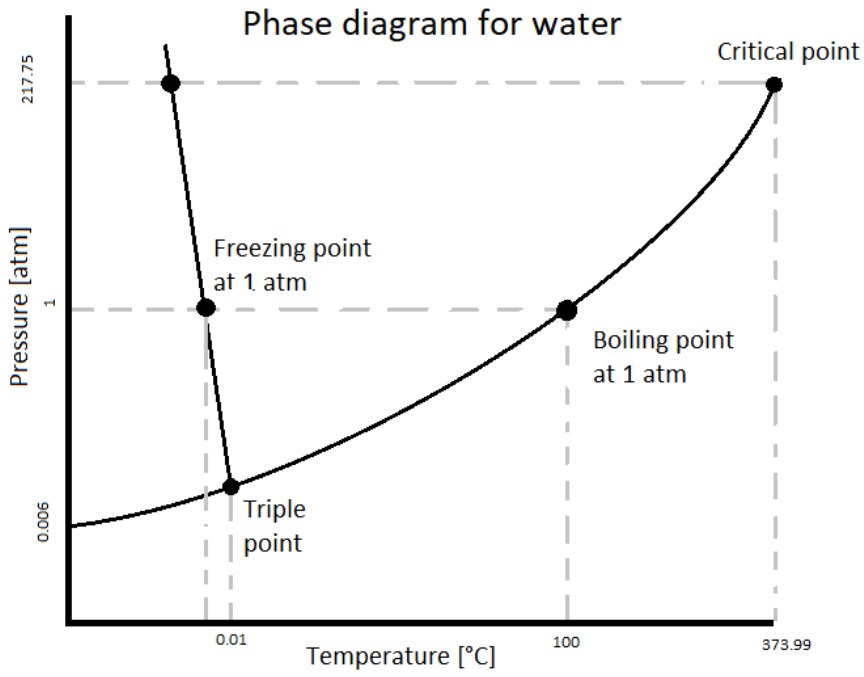

Figure 4.1. Phase diagram of water [14]

The seemingly exponential boiling point line is a visual representation of the behavior of $\frac{dP}{dT}$ from equation 4.3

It is still important to note that the temperatures used in equation 4.2 refer to those at the membrane's respective surfaces, not in the bulk. This prevents direct measurement of the value.

These equations work well for ideal solutions of pure water on both sides of the membrane, but for highly saline or polluted solutions some modifications have been performed:

$$J = C_m \frac{dP}{dT}[(T_f - T_p) - \Delta T_{th}](1 - x_m) \tag{4.6}$$

where T_{th} describes the threshold temperature, which is given by:

$$\Delta T_{th} = \frac{RT^2}{M_w \Delta H_v} \frac{x_f - x_p}{1 - x_m} \tag{4.7}$$

where x_m, x_f, x_p represent mole fractions of dissolved species in-, on the feed side of-, and on the permeate side of the membrane, respectively. This is only relevant for extremely salty streams, or if very precise measurements must be made.

Equation 4.6, by Schofield et al. suggested that this modification was to account for lower vapor pressure as a result of dissolved species in water. [15]

The mechanism of the mass transfer itself can be divided into 3 possible models. Depending on the size of the membrane's pores, the transport mechanism will be dominated by collisions of different types. For small pores, the dominant collision type will be between water vapor molecules and the pore wall, for large pores molecular collisions will be dominant, and there exists a sizing in which co-dominance will occur. The former is named Knudsen diffusion, and this occurs when the mean free path of the molecules is significantly larger than the size of the pores, meaning that molecule-wall collision will be the dominant transport mechanism. The mean free path is described according to the kinetic theory of gases, and as such the molecules can be estimated as hard spheres that engage only in binary collision. [8] The equation for mean free path length is shown below:

$$\lambda = \frac{k_B T}{\sqrt{2}\pi P d_e^2} \tag{4.8}$$

where λ is the mean free path, k_B is the Boltzmann constant, T is absolute temperature, P is the mean pressure inside the membrane, and d_e is the diameter of the molecule. [8]This mean free path can be calculated for a given temperature, and compared to the average expected size of the pores, making it possible to assess which form of transport should be dominant.

In the Knudsen region, where the pore's inner diameter is smaller than the mean free path (i.e. $d_P < \lambda$), Khayet et al. [16] pointed out that the membrane coefficient for operating under such conditions can be described as:

$$C_{Kn} = \frac{2\pi}{3}\frac{1}{RT}\left(\frac{8RT}{\pi M_w}\right)^{\frac{1}{2}}\frac{r^3}{\tau\delta} \tag{4.9}$$

where τ, r and δ are pore tortuosity, -radius, and membrane thickness respectively.

In the contrary scenario, when the pore size is enormous compared to the mean free path (i.e. $d_P > 100\lambda$), the ordinary molecular diffusion theory overtakes the transport mechanism completely. Under such circumstances, the membrane coefficient can be described as:

$$C = \frac{\pi}{RT}\frac{PD}{P_{air}}\frac{r^2}{\tau\delta} \tag{4.10}$$

Where P_{air}, P, D are air pressure within a membrane pore, total pressure inside the pore (equal to air and water vapor pressure combined), and diffusion coefficient respectively.

In the transition region ($1 < \lambda < 100$), both mechanisms play a significant role in the overall mass transport mechanism. [16] As there are multiple mechanisms at work, the

equation has aspects of a linear combination dependent on pore size, but ends up being somewhat unintuitive compared to the models where a single mechanism dominates:

$$C_c = \frac{\pi}{RT}\frac{1}{\tau\delta}[(\frac{2}{3}(\frac{8RT}{\pi M_w})^{\frac{1}{2}}r^3)^{-1} + (\frac{PD}{P_\alpha}r^2)^{-1}]^{-1} \tag{4.11}$$

Where the diffusivity of water through the air inside the pores (PD) can be expressed as:

$$PD = 1.895 * 10^{-5}T^{2.072} \tag{4.12}$$

Some authors [17] believe permeate flux is higher when approaching the critical pore size, in which Knudsen diffusion is dominant, as opposed to the transition region.

4.1.2 Heat transfer

In MD, two fundamental mechanisms for heat transfer are significant: Latent heat-, and conduction heat transfer. [18–20] Generally, the transfer can be divided into 3 sections: convection from feed bulk to membrane, latent heat of vaporization at the liquid/vapor interface, and convection from membrane to permeate. [8] The first process that occurs is the convection of heat from the feed bulk into the membrane, this can be described as follows:

$$Q_f = h_f(T_f - T_{f,m}) \tag{4.13}$$

Where Q_f is heat flux of bulk to membrane, h_f is the feed water's heat transfer coefficient, and T_f and $T_{f,m}$ is the respective temperature of feed bulk and the feed side of the membrane.

Next, the latent heat of vaporization transfers heat through the membrane, and it can be described as:

$$Q_m = h_m(T_{f,m} - T_{p,m}) + J\Delta H \tag{4.14}$$

where Q_m is the latent heat flux, h_m is the membrane heat transfer coefficient, and $T_{f,m}$ and $T_{p,m}$ represents temperatures at feed- and permeate sides of the membrane respectively.

As one might expect, the final part of the heat transport mechanism is the convection transport of heat from the membrane on the permeate side into the permeate bulk, this can be expressed as follows:

$$Q_p = h_p(T_{p,m} - T_p) \tag{4.15}$$

Where h_p is the heat transfer coefficient of the permeate.

Often systems will operate under steady state, where both the feed and permeate are kept at set temperatures. Under such circumstances, the overall heat flow (Q), also remains the same. This effectively means that all three mechanisms will have the same flow:

$$Q = Q_f = Q_m = Q_p \tag{4.16}$$

This effectively means that the slowest of the three mechanisms will become to overall heat transfer of the system. Equation 4.16 can thus be written as:

$$Q = U(T_f - T_p) \tag{4.17}$$

Where U represents the total system heat transfer coefficient. For high operating temperatures, (i.e. high temperature gradient) the most significant factor will be the latent heat transfer. [19] This is due to the increased mass flux of those conditions, bringing more latent heat into the permeate side of the membrane.

As discussed previously in this section, direct measurements of temperature on either face of the membrane is experimentally impossible. This has lead Termpiyakul et al. [21] to develop an iterative mathematical model to approximate temperatures based on bulk readings:

$$T_{f,m} = T_f - \frac{J\Delta H_v + \frac{k_m(t_{f,m} - t_{p,m})}{\delta_m}}{h_f} \tag{4.18}$$

$$T_{p,m} = T_p - \frac{J\Delta H_v + \frac{k_m(t_{f,m} - t_{p,m})}{\delta_m}}{h_p} \tag{4.19}$$

By first inserting T_p and T_f in the places of their respective membrane-surface counterparts, and through a series of repeated iterations, good estimates of $T_{f,m}$ and $T_{p,m}$ can be made. In systems with high crossflow velocity, however, these iterations often lead to no significant change as the diffusion layers will be very small. [22]

Temperature polarization

Alkhudhiri et al. [8] describe temperature polarization as the temperature difference between the liquid/vapor interface and the bulk:

$$\psi = \frac{T_{m,f} - T_{m,p}}{T_f - T_p} \tag{4.20}$$

where ψ is the temperature polarization. Lawson [23] pointed out that for VMD equation 4.20 should be written as:

$$\psi = \frac{T_f - T_{f,m}}{T_f - T_p} \tag{4.21}$$

Polarization is most relevant at high temperatures and/or low feed velocity.

4.2 Wettability

It has been mentioned in this work that for a membrane to function for MD purposes on systems with aqueous solutions it must be hydrophobic. Strong hydrophobicity makes it less likely for the membrane to enable transfer of the liquid phase through the pores directly, in what is known as wetting. [8]

When discussing wetting, the Young equation describes the system as follows:

$$\gamma_{sl} + \gamma_{lv} cos(\theta) = \gamma_{sv} \tag{4.22}$$

Where $\gamma_{sl}, \gamma_{lv}, \gamma_{sv}$ are the interfacial tensions between solid/liquid, liquid/vapor, and solid/vapor respectively. θ is the contact angle, measured in degrees. [24] It is generally accepted nomenclature that if the contact angle is between 0° and 90°, the material is hydrophillic, and between 90° and 180° it is hydrophobic. When the tensions are higher between the solid/vapor interface than the solid/liquid interface (i.e. when $\gamma_{sv} > \gamma_{sl}$ wetting occurs; if the opposite is true, non-wetting occurs. Furthermore, if the difference in tension between the solid/vapor and the solid/liquid is greater than the liquid/vapor interface, the liquid will be absorbed into the membrane to avoid interacting with the vapor, and no droplets can form on the surface. While Young's equation 4.22 is theoretically accurate for a flat membrane surface where surface topology is to be ignored, Wenzel found it necessary to make an adjustment to account for surface roughness [25]:

$$cos\theta^w = r\frac{\gamma_{sv} - \gamma_{sl}}{\gamma_{lv}} \tag{4.23}$$

Where θ^w is the observed contact angle and r is the roughness parameter, essentially a correction term for rough surfaces that follow the Wenzel equation. It is interesting to note that in the Wenzel equation 4.23, the material's inherent tendencies are amplified by roughness, meaning hydrophobic surfaces will becomes increasingly so at higher roughness, while hydrophillic materials become more hydrophillic. This is because Wenzel describes the roughness as simply an increase in area of interaction, meaning all interactions, favorable or unfavorable take place at a higher density on a rough surface than a smooth one. [25]

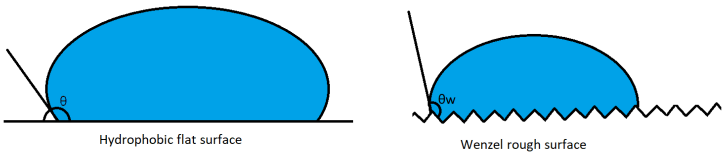

Figure 4.2. A droplet on a hydrophobic flat surface (left) and a droplet on a rough surface (right), displaying some of the difference between Young's and Wenzel's theories. [25]

Figure 4.2 illustrates the difference between the suitable situations for Young's and Wenzel's equations respectively.

For a membrane to wet, the liquid entry pressure (LEP) must be exceeded.

$$\Delta P = P_f - P_p = \frac{-2B\gamma_i cos(\theta)}{r_{max}} \tag{4.24}$$

Equation 4.24, as described by Franken et al. [26], shows the basic equation to describe hydraulic pressure difference, ΔP, over a membrane. P_f and P_p are pressures on feed and permeate sides respectively, B is a pore geometry coefficient (1 is usually used for cylindrical pores), and r_{max} is the maximum pore size. For the material to wet, the pressure difference must exceed the critical LEP, i.e. $\Delta P > LEP$ must be true for the membrane to wet.

4.3 Surface modification of ceramic membranes

Pristine ceramic membranes are not suitable for MD, as they are typically hydrophilic and have large pores. [27] These factors allow the membrane to be wetted by aqueous solutions upon contact, preventing separation of pollutants smaller than the membrane's pore size from occurring. Still, ceramic membranes have some considerable advantages over polymeric membranes in terms of both thermal and chemical strength. [27] Therefore, scientific interest in procedures for surface coating on ceramic membranes to improve hydrophobicity and repel water has been high. An example of such a study is Boffa et al. who treated a silicon carbide (Si-C) membrane with a Fluorinated Polyhedral Oligomeric Silsesquioxane (F-POSS) to achieve a superhydrophobic surface coating and run MD despite the natural hydrophillicity of the Si-C membrane. [28]

In many cases, these syntheses are based on a type of sol-gel reaction, by which small particles of silica are formed and then grafted onto the membrane. [29, 30]

4.3.1 Sol-gel

Sol-gel may refer to the preparation of nanoparticles of silica by hydrolosis and condensation reactions from alkoxysilanes in a mixture of water, ethanol, and ammonia. [31] This is known as the Stöber process. The size and distribution of these particles will vary, and is quite sensitive to the conditions under which they form.

The application of grafting these particles onto surfaces is two-fold: they add micro roughness, which inherently makes the surface repellent, and they allow further surface modifications, as these silica particles present alcohol groups that can be modified easily. [31, 32]

4.4 Semiconductors

Semiconductors are a class of materials that fall between metals and insulators in terms of their electrical conductivity. The electrical conductivity can be expressed in the form of a material's band-gap; materials with a higher band gap will have lower electrical conductivity. For semiconductors, it is commonly accepted that the bandgap be between 0 and 4 electron volts (eV). [33]

When metals or nonmetals form crystals, their orbitals may considerably overlap. This causes a splitting of the individual orbital energies of the single atoms. As the lattice grows, this may lead to the formation of a continuous band. In this context it is suitable to introduce the band gap as the energy difference between two distinct bands: the valence band (VB) and the conduction band (CB). The VB represents the most energy rich orbitals that still have electrons present, while the CB is the least energy rich orbital band that does not contain electrons. This means that $CB > VB$ in energy, and the value of this gap measured in eV determines if the material can be considered a conductor, a semiconductor or an insulator. [34, 35]

The use of semiconductors in the context of this work is as a material which can produce electricity, and as such, the most interesting property is photo excitation. [36] When photoexcitation occurs, an electron shifts from the VB to the CB as a result of an outside photon striking the atom. The electron then goes to a higher energy state, leaving behind a hole. To return to the ground state, the electron must return to the VB leading to their annihilation, in a process referred to as recombination. Simple relaxation by photon emission would return the VB to the status quo, but it is also possible to separate the charges with recombination occurring externally, and this is what may drive a photoelectric current in the process.

4.5 photovoltaics

In intrinsic semiconductors, like pure single crystal silicon, recombination through relaxation will be the exceedingly abundant mechanism for returning to the ground state. However, it is possible to dope the material to enhance charge separation,as was first achieved in 1941 with natural defects. [9, 36] In the silicon PVs of today, this doping is done with Boron and Phosphorous to make P-N junctions. For inorganic photovoltaic devices the same intrinsic semiconductor (i.e. a silicon lattice) can be used on both sides of the junction, with different doping elements to create the junction.

The overall mechanism is relatively simple: when sunlight strikes the PV, photons of certain wavelengths are absorbed by the active silicon layer, and an electron is elevated from the ground state. Upon its dissociation, the negative electron and the positive -hole will travel away from the junction to the n- and p type regions respectively. By adding electrodes to either side of the active layer, the induced potential can be exploited for work in the form of a current. [36]

Due to spectral mismatch, recombination through relaxation, and heat generation within the cell, it is estimated that the theoretical PCE limit of single crystal silicon-based PVs is around 34.37%. [37] This means the remaining 65.6% of the total energy are either reflected as photons after impact or retained as heat in the cell. That said, current cells have a much lower PCEs, with the current market for single crystal Si-PV at a PCE of $<25\%$, leaving $>75\%$ of the total energy unused in the form of relaxation or retained heat.[37]

To release an electron from the lattice, a given photon has to have sufficient energy. In silicon, this threshold is roughly 1.1eV, translating to a wavelength of roughly 1100nm [38]. This means any radiation with a lower energy i.e. higher wavelength than this will instead

cause vibrations that will heat up the lattice. Moreover, photons of higher energy will not dislodge more electrons; any excess energy will be emitted as a photon upon collision, which will further cause the material to heat up. These phenomena are what causes the theoretical limit PCE of Si-PV.

Maksymov et al. [39] highlight the AM1.5 solar spectrum, which shows strong intensity in the 400-1150nm range, where Si-PV's are quite active, showcasing that the potential for power conversion from solar radiation is high for Si based PV systems.

It has been previously mentioned how a cell of high heat retention will experience increased operational temperatures, leading both to a loss of PCE and loss of lifetime due to lattice degradation. The reason for this is a combination of increased vibrational stress in the lattice, causing increased electrical resistance, and the junction losing its power to effectively separate charges as temperature increases. [38] At standard operating temperatures, the former of these effects will be the primary reason for reduction in PCE in silicon PV cells. More specifically, these effects reduce the open circuit voltage significantly, leading to a reduced potential for work. [40] The short circuit current, at which there is maximum current but no voltage, remains almost if not exactly in place at different temperatures. Contrarily, open circuit voltage, at which there is maximum voltage but no current, decreases substantially. This results in reduced efficiency, as the amount of work that can be extracted, that is to say P_{max} in the PV decreases noticeably with temperature. [40]

If temperatures of 300°C are reached, the electrons and -holes would have so much energy that they could pass the junction as if the barrier was not present, eliminating the potential difference and effectively short-circuiting the cell over the junction. [38] The induced higher operating temperature also creates a feedback loop: the lowered PCE means that less energy leaves the cell as usable electricity, and so the flux of trapped energy necessarily increases, further increasing operating temperature. This continues until a balance is struck between the black body radiation and the heating mechanism from within the cell; this typically leaves the cell at around 60°C under direct solar radiation.[13]

5 Experimental Considerations

To perform experiments to investigate the PV-MD combination, a module to hold water and a membrane for MD had to be created. Likewise, a small PV panel had to be obtained.

5.1 Water module

The panel obtained had dimensions of 8- by 14 centimeters. Initially, it was attempted to create a container that would wrap around the panel, this was done by using 3D printing. This module had an inside water volume of close to 100mL, and a pre-placed hole on one of the short 8cm surfaces to allow for a thermometer. The purpose of this equipment was to investigate the steady-state temperatures attainable within the case and use that value as a baseline for temperatures of feed in the MD part. This idea had a number of flaws, both on the experimental and the theoretical side. i) disconnecting the PV heating and the MD application means any data on steady state conditions will ignore the latent heat transfer from the vaporization and subsequent transportation of heat over the membrane. ii) the available sun simulation lamp had a spot of 5cm diameter, meaning that constructing a case that holds 100mL and stores water evenly behind the entire area of the PV panel is redundant and the total water volume far too large to bring up to useful MD temperatures. iii) Having only one hole, filling the module was often difficult due to the potential of trapped air.

To address all of these issues, the module was redesigned to both decrease volume and active area, as well as incorporate the membrane directly in the design. This meant that two new pieces had to be 3D printed, one to hold water and attach an adequately sized flatsheet membrane, and one to act as permeate side of the module. With a smaller volume of about 20mL, placed behind only part of the PV panel, it would be reasonable to assume higher temperatures could be reached, whereby mass transport through the membrane should be enhanced. Both the pieces were also printed with 3 pre-placed holes, to allow for the potential of DCMD and a thermometer in each chamber. This second version was originally designed to rely on tape to seal the module, but this quickly proved unfeasible both due to the timescale of experiments as well as the force of the vacuum that would need to be applied in VMD.

Subesquently, a third version was created. This model was designed with O-rings in mind for both components, sealing the membrane between the layers of O-ring and compressing the rubber with screws and bolts on both sides. The hope with this model was to increase the robustness of the system to effectively seal the water chamber and prevent leaks. This module was printed in acrylonitrile butadiene styrene (ABS) plastic for its thermal stability,

but during experiments cracks started forming due to over stress from the screws. Initially, an attempt was made to combat this issue with parafilm, and subsequently by wetting the cracked parts of the module in acetone, as it would soften the polymer and potentially close the cracks. Attending the problem this way proved futile, as the aforementioned solutions would only prolong leakage somewhat, and not enough for the module to remain useful for experiments. This meant an additional print had to be made, with both material choice and module chassis dimensions adjusted.

The fourth module came with the following adjustments

- The ridge between the water chamber and the O-ring was extended by 2mm to increase strength.
- The depth of the grooves was reduced by 1mm, so less pressure was necessary to seal the membrane between O-rings.
- The outer walls were adjusted in size, making the entire module wider.
- Screw-holes were moved further away from the groove to reduce chances of crack propagation into the groove which destroyed the previous model.
- Print material was changed from ABS to acrylonitrile styrene acrylate (ASA) to increase toughness against fractures.
- The bottom chamber was designed with a large hole designed to integrate a fitting for a vacuum tube.

The overarching design idea of O-rings sealing the membrane in between the chambers and screws and bolts for compression remained the same however, and a picture can be seen below on figure 5.1:

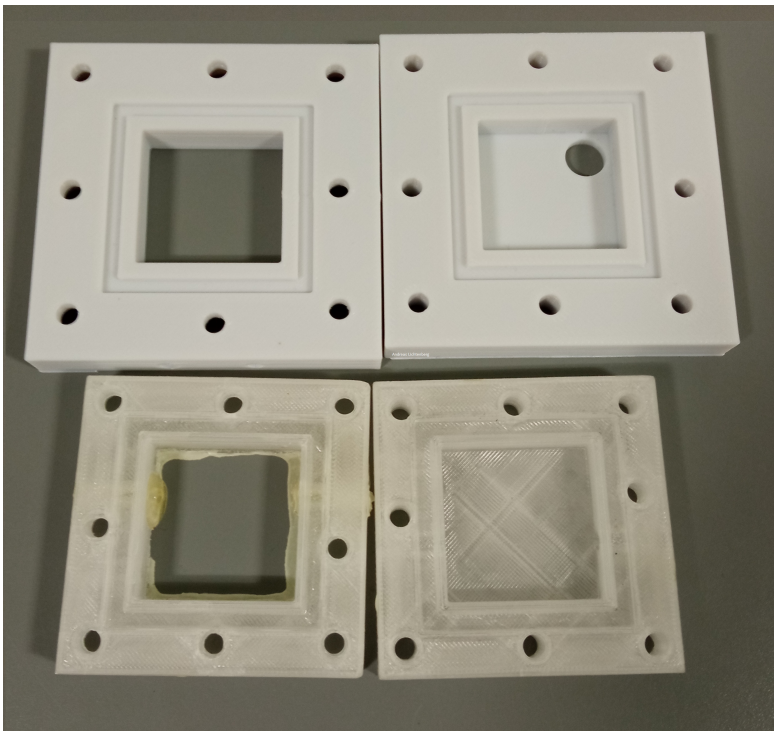

Figure 5.1. image of module model 4 (top) and -model 3 (bottom)

This print proved stronger, as no visible cracks formed and the module maintained the ability to seal the water in the feed chamber. To adjust for new and slightly thinner O-rings, the O-ring placed against the membrane's support layer was wrapped in parafilm to allow extra compression and help sealing the module. The reason this was only done on the support side is that the active polytetrafluoroethylene (PTFE) layer would readily stick to the parafilm and peel off the support, ruining the membrane piece. In experiments where the temperature was expected to rise above 50°C, the parafilm was changed in favor of teflon tape to prevent the parafilm from liquefying and ruining the experiment. A small fitting was printed to connect the permeate chamber to a vacuum pump. As such, it was important to also incorporate a mesh structure to place in between the bottom of the permeate chamber and the membrane, so as to not tear the membrane apart when the vacuum was pulled. This mesh was also 3D printed. The fitting was glued in place to seal properly, and the mesh was simply placed in the chamber before closing the module.

5.2 Choice of experiments

With a functioning module in place, the experimental run could be planned. The goal was to investigate how effective the design was at performing membrane distillation as well as keeping the open circuit voltage of the panel higher over a longer period. Therefore, it was paramount to have a baseline experiment, where no membrane distillation took place and the panel operated as it would without the cooling system. Once done, future experiments could be compared to this baseline to investigate effectiveness of different system setups.

Experiments under the first 2 sets of conditions were run both with artificially salted water (35g/L sodium chloride solution) and pure water. This was to gain an understanding about how the system would behave with different feed solutions. It was hereby observed that the system behaved predictably according to theory, and that the primary factor for the observed flux decrease in the more saline solution was the increase in the enthalpy of vaporization. After this was established, further experimental conditions focus on the application of supplying sea water or slightly polluted streams to the feed, and so the feed solution used is artificially salted.

Given the 0.1g resolution on the scale used in these experiments, experiments were run on a higher irradiance than normal sunlight. Traditionally, sunlight has an irradiance of around 1000 $\frac{W}{m^2}$, but to ensure data would be produced from the scale, experiments were conducted at an irradiance of 1850 $\frac{W}{m^2}$

5.2.1 Vacuum setup

The simplest setup used had the panel with the module attached, a reservoir on a scale, and the sun simulation instrument shining on the panel, so the 2 cells in front of the MD module were fully illuminated. The addition of a vacuum pump and some tubing was quite simple, and can be seen below on figure 5.2:

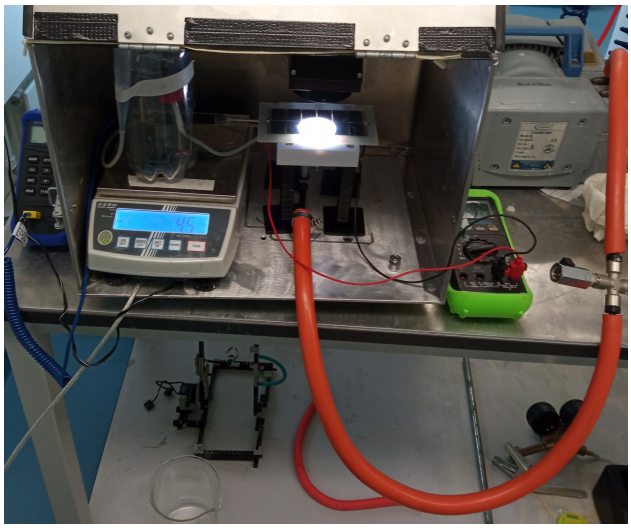

Figure 5.2. Simple setup with orange vacuum tube featuring a valve and barometer.

In all experiments performed at a vacuum, the pump was turned on after 1 hour had elapsed. This was due to very low observed temperature prior to the 1 hour mark due to a poor heat transfer from PV to feed. While turning the pump on at the start surely would have lead to a flux that would very likely follow the known MD theory, it was regarded as inefficient and therefore irrelevant.

5.2.2 Heated reservoir

After having performed the previous runs of salt and pure water, both as AGMD and VMD, it was worth exploring how the panel would perform if the temperatures became more favorable for MD. This setup essentially simulated a system in which panel efficiency is disregarded in favor of maximum MD performance, and the expectation was that the open circuit voltage would both start and end considerably lower than seen before. The entire system was rebuilt to now feature a much larger reservoir to account for the increased dead volume of more tubing, a peristaltic pump and a hot water bath on a hotplate with a metallic coil through which the feed water was pumped. The modified part of the setup can be seen below in figure 5.3

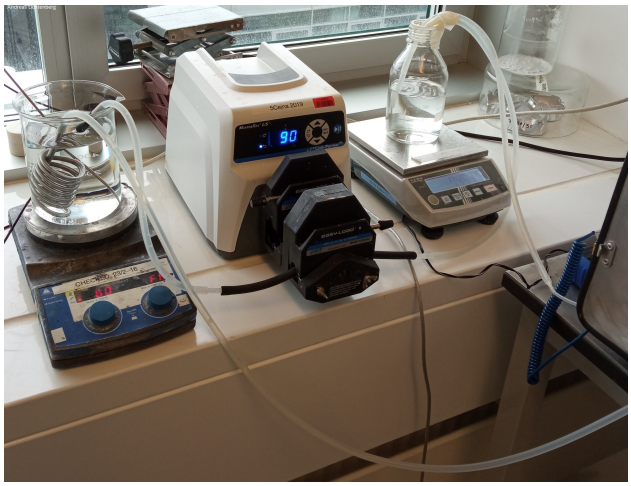

Figure 5.3. The rebuilt system with active heating

The target feed temperature for these experiments was 60°C, as this has been shown to be the steady state temperature of PV cells under continued operation for extended periods. [13]

5.2.3 Heat sink modification

Previous experiments had lead to a steady state temperature of the feed solution of around 33-35°C. A similar study from 2021 by Antonetto et al. [41] showed considerably higher temperatures when performing their experiments. It was therefore clear that efficiency of heat transfer could be improved considerably by the addition of a metallic heat sink to the back of the panel. As such, 2 pieces of aluminium were glued to the back, and another 4 were subsequently attached to those to more effectively disperse heat into the feed water. AGMD and VMD experiments were then conducted with this modification also in place.

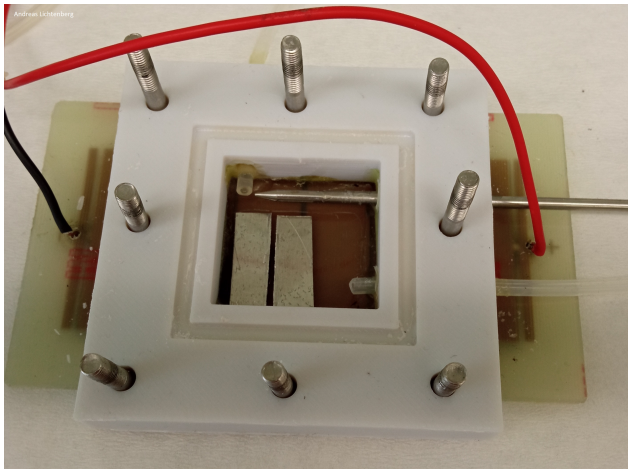

Figure 5.4. The feed chamber with the first part of the heat sink installed

Figure 5.4 shows the panel's back plate, the module's feed chamber, and 2 pieces of aluminum glued to the back plate to enhance heat transfer.

5.3 Statistical analysis

A small statistical analysis of the 5 first experiments was conducted. These had some differences in their setup, namely that 2 experiments were VMD, 2 were AGMD, and one was a baseline with no water present at all. The reason these experiments were grouped was that the further experiments - meaning the experiments with a heated reservoir or a heat sink installed - were expected to show significantly different results. It was therefore important to have a comparison more thorough than a baseline with no true way of knowing how extreme future results were compared to the expected values. However, there are some noticeable problems with conducting the analysis on these 5 different experiments; for example the claim that these experiments should come from the same population is dubious, as there were setup changes between them.

Using these 5 experiments to estimate flux would be impossible, however, as the runs described are clearly far too different in this metric to produce anything meaningful. Therefore, only open circuit voltage and temperature were taken into consideration.

The calculations were quite simple: for each timestamp, the average data point and the variance of each value compared to this average was calculated. Then, the standard deviation of that particular timestamp was calculated, and thus an upper and lower bound for the expected value could be generated, plotting the average $\pm$ 1.96 standard deviations. This meant any data that fell outside this range could, with 95% confidence, be considered a significant change.

5.4 Ceramic module

The ceramic membranes were prepared in following the procedure of Nielsen [42], who modified the procedure presented by Yang et al. [31] The module was assembled with fittings to allow the tubes previously used in such a way that there was a small cavity before the membrane to allow for a thermometer. After the module was assembled, the initial test revealed that both membranes would wet almost immediately. The tubes were then rewired so the membranes were in separate streams, and tested individually. This test seemed to confirm both membranes wetted but with noticeably different flow rates. It was then decided that both membranes would be tested as flow regulating devices for a traditional water cooling device, simply by extracting thermal energy from the PV along the stream. The difference in flow rate would hopefully provide some interesting insight into ideal configuration for a system relying on this technique.

6 Procedure

6.1 Photovoltaic-Air Gap Membrane Distillation experiment

The module was assembled by attaching the 3D printed feed chamber and screws to the back of the PV panel with epoxy, in such a way that 2 cells were fully covered from behind. 4mm silicon tubes were fitted into the holes in the print design for water inlet and outlet. This was then also fastened with epoxy. Then, the O-rings were put into place in both the feed- and permeate chambers, and the membrane was placed in between. A reservoir was attached to the inlet and placed on a data acquisition scale inside a light excluding metal box with the LOT Quantum Designs sun simulation beam inside. A Tecpel™ thermometer was inserted into the feed chamber. the panel's built-in wires were connected to a voltmeter to continuously measure open circuit voltage during the experiment. 50mL of either distilled- or salted ($35g/L$ sodium chloride) water was then added to the reservoir and the lamp was turned on with an irradiance of 1850 $\frac{W}{m^2}$. Weight data was collected at 300s intervals, and the temperature- and voltage measurements were manually taken at 30 minute intervals. Total experimental time was 4 hours.

6.2 Photovoltaic-Vacuum Membrane Distillation experiment

A 3D printed fitting was installed in the module's permeate chamber. This fitting could be attached to a vacuum pump through a series of adapters, also allowing for a valve and a barometer along the tube to the pump. The experiment was initiated the same way as before, except at the 1 hour mark the pump was turned on and the valve was closed over the following 2 minutes to smooth the pressure curve and prevent sudden stresses in the module. Data aquisition, measurements, and total experimental run time were all unchanged.

6.3 Artificially heated Air Gap- and Vacuum Membrane Distillation experiments

The module assembled as described in section 6.1 was attached to additional tubing leading through a metallic spiral placed in a full 2L beaker kept at 60°C by a hot plate and a peristaltic pump. The reservoir was increased in volume to 500mL and the scale was

moved outside the light excluding box. The peristaltic pump and heater were turned on, and when the water in the bath was at 60 degrees, the experiment was started as before.

6.4 Water cooled Photovoltaic experiment with modified ceramic membrane

The module was assembled in a number of stages. Initially, the coated membrane was cut in half to create 2 half-circles. These were then attached to fittings on each end with epoxy to allow for tubing to connect to the reservoir. Onto these fittings, another 3D printed piece was added, making a half-circle shape to allow for the chamber to be closed with a cut half-circle piece of Plexiglass. This plexiglass semicircle was previously equipped with a 3D printed vacuum tube fitting. Once this module was shown to hold water as intended, it was attached to the panel as before. Experimental procedure remained unchanged: 4 hour run time under 1850 $\frac{W}{m^2}$ irradiance. A beaker was placed underneath the fitting to catch the flow of salt water from the membranes.

7 Results and Data Analysis

7.1 I-V diagram

The I-V diagram for the panel used in this work was created using two multimeters, the panel, a variable resistor, and an irradiance measuring device. The panel was connected to the first multimeter to measure voltage, the other was then connected to those same wires and the variable resistor to measure current. The resistance was then varied and data was acquired and plotted into an I-V diagram.

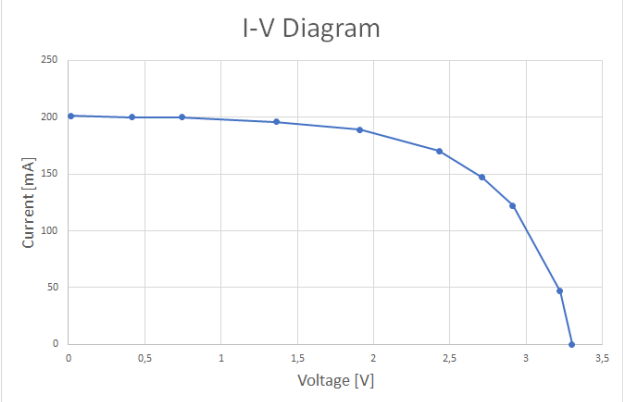

Figure 7.1. I-V diagram of panel used

The diagram shows a short circuit current of around 200mA and an open circuit voltage of 3.3 Volts. As mentioned in section 4.5, the fill factor is described by the ratio between the area of the largest square inside the curve and the square that can be drawn between the short circuit current and open circuit voltage.

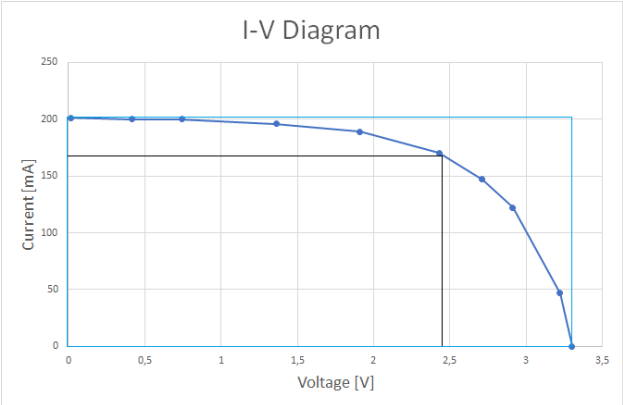

Figure 7.2. I-V diagram with fill factor displayed

Calculating the ratio between the areas of these squares yields a fill factor of about 0.61. the PV's PCE may be calculated as $\frac{V_{oc}*I_{sc}*FF}{I_{rr}}$. Knowing the radiation density G was around 1200 $\frac{W}{m^2}$ for this experiment and the cell area was 0.005 M^2, P_{in} may be calculated as $G * A$.

$$\eta = \frac{V_{oc}I_{sc}FF}{P_{in}} \tag{7.1}$$

Performing this calculation yields a PCE of 6.2%.

7.2 polymeric membrane PV-MD experiments

7.2.1 Baseline experiment

The baseline experiment was performed with the intent of revealing to whether operation of AGMD or VMD respectively could slow down or stop the decrease of open circuit voltage as a result of increased temperatures.

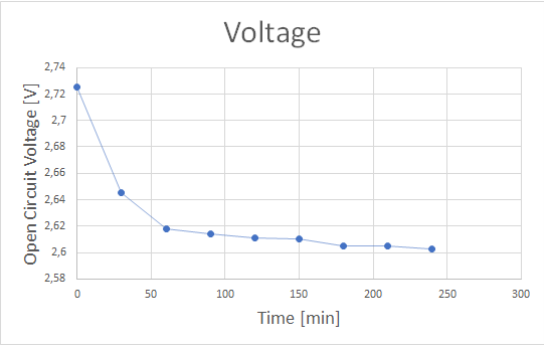

Figure 7.3. Open circuit voltage of PV measured over 4 hours with no MD

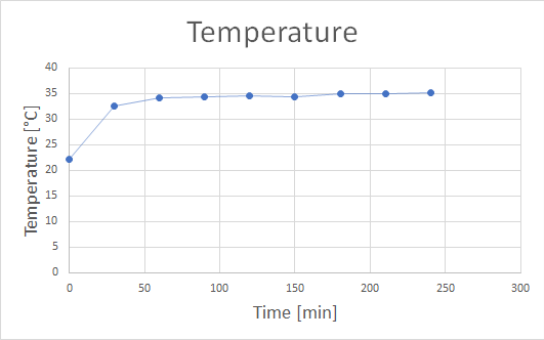

Figure 7.4. Temperature inside module measured over 4 hours with no MD

These figures show an expected drop in open circuit voltage in figure 7.3 as well as an increase in temperature behind the panel in figure 7.4. As expected, these values are both

asymptotic with time - they reach limit values as the system stabilizes. The success of further experiments will in part be judged based on how they adjust these asymptotic values, i.e. to what extent open circuit voltage can be increased at steady state, and how much temperature in the cells can be lowered. The latter, is not directly measured, rather open circuit voltage and temperature in the feed chamber are used as proxies.

7.2.2 AGMD experiments

Pure water

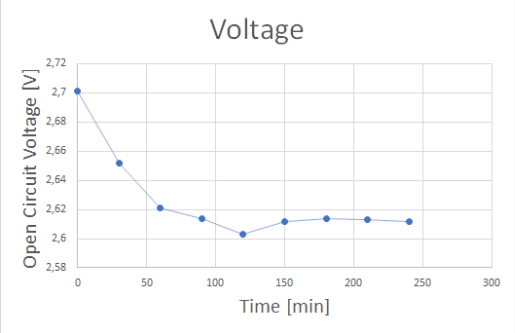

Figure 7.5. open circuit voltage of PV measured over 4 hours with distilled water in the module

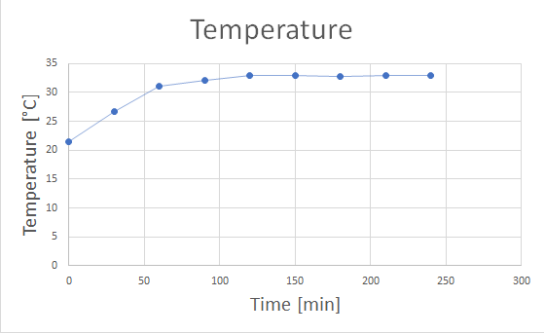

Figure 7.6. Temperature of water in the module over 4 hours with distiller water

Figures 7.6 and 7.5 show the same information as before, but on the experiment with distilled water in the module. Open circuit voltage appears to develop in a very similar manner as the blank, whereas the temperature is shown to be slightly slower to reach an also lower steady state value.

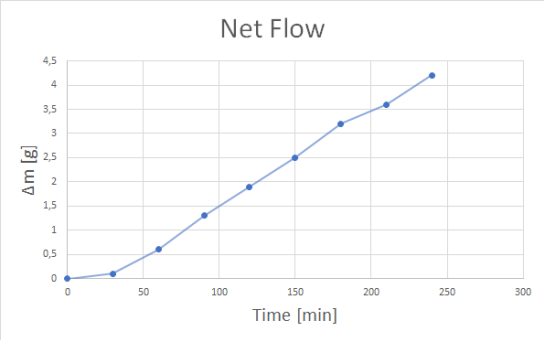

Figure 7.7. Net flow over the experiment

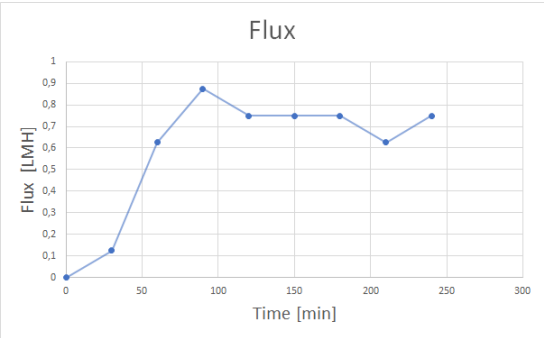

Figure 7.8. Calculated flux in LMH over the course of the experiment

The last interesting aspects for this experiment are flow and flux as depicted in figures 7.7 and 7.8 are the observed flow and flux that can be attributed to membrane distillation occurring in the module. Notably, it takes about an hour to reach what can be considered steady state for the system, as both flow and flux stabilize around this moment. Flux in this work will be displayed as liters of distillate pr. square meter membrane area pr. hour

(LMH). Flux of this experiment is calculated at an average of 0.66 LMH overall, and 0.75 LMH in the last 3 hours.

Salt water

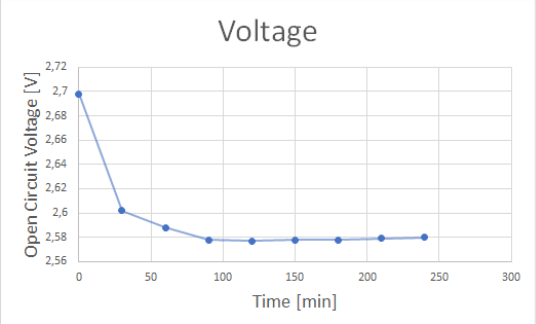

Figure 7.9. Open circuit voltage of PV measured over 4 hours with salt water in the module

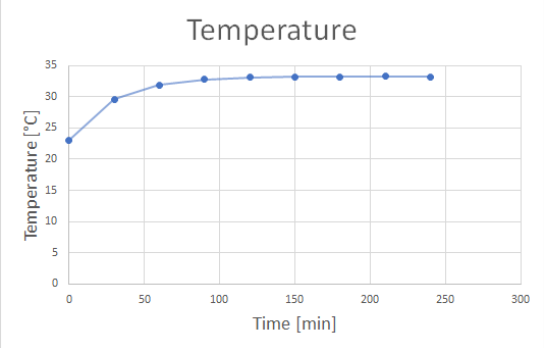

Figure 7.10. Temperature of water in the module over 4 hours with salt water

The observed drop in voltage over the course of this run was similar to the blank, at about 0.12V, however the temperature stabilization remained more in line with the pure water experiment at 33.2°C.

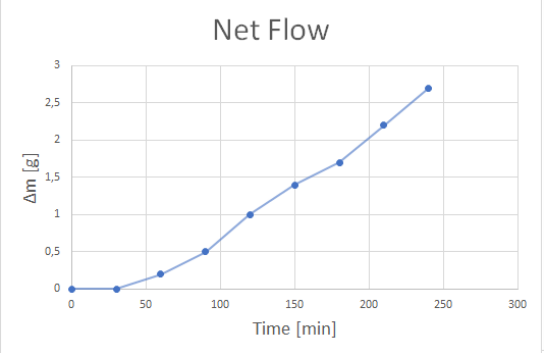

Figure 7.11. Net flow over the experiment

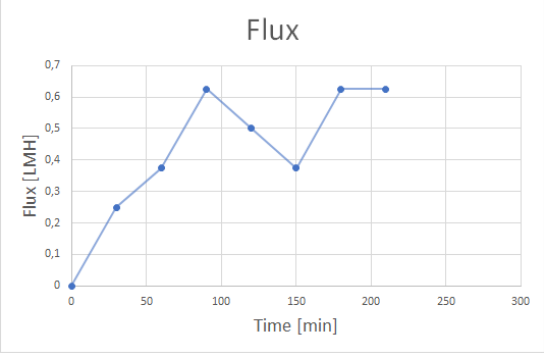

Figure 7.12. Calculated flux in LMH over the course of the experiment

The flow observed in this experiment was somewhat lower that than without salt according to data from the weight. It was expected that flux would be slightly lower due to the lower vapor pressure as well as higher heat enthalpy of vaporization for salty solutions. The average flux over the course of the whole experiment was calculated to 0.42 LMH and 0.55 LMH neglecting the first hour.

7.2.3 Vacuum MD experiments

Pure water

To investigate the impact on flux and steady state temperature, the permeate chamber was fitted with a vacuum tube, and a pump was turned on after 1 hour. The pressure in the

permeate chamber was measured with a barometer placed between vacuum tubes which also included a valve so the vacuum could be applied steadily to avoid pressure shock. The pressure remained at 0.2 bars after the pump was turned on.

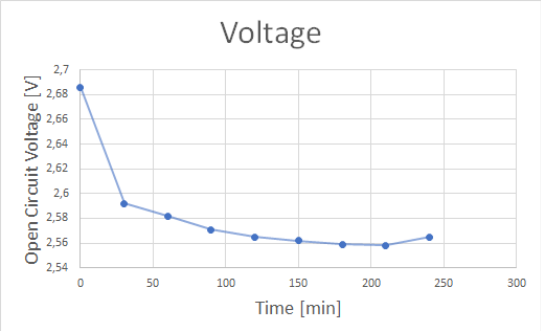

Figure 7.13. Open circuit voltage over the 4 hour run time

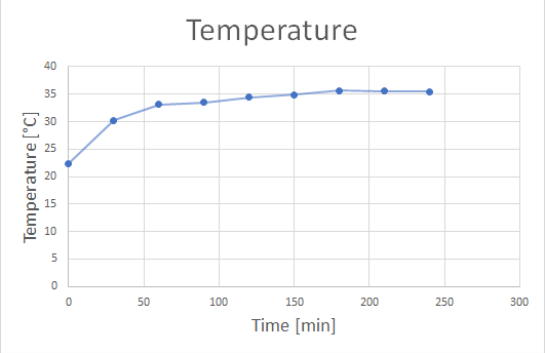

Figure 7.14. temperature behind the panel over the 4 hour run time

The steady state temperature reaches a higher value than that in prior experiments, indicating that the heat transfer is better under these conditions, as the increased flux should lead to more cooling.

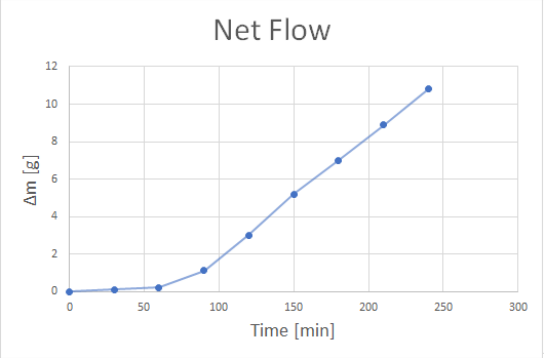

Figure 7.15. Net flow over the experiment

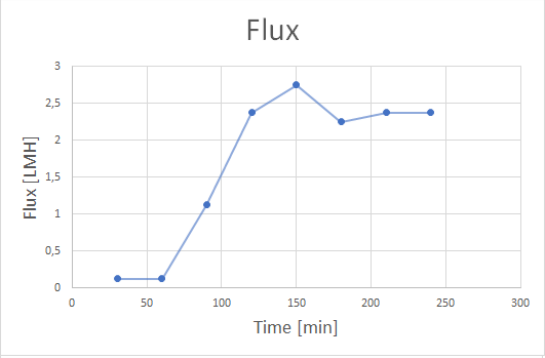

Figure 7.16. Calculated flux in LMH over the course of the experiment

Using equations 4.1 and 4.5, as well as the data from previous AGMD experiments, flux at a vacuum was estimated to be around 2 LMH for a full vacuum. The flux data in this run matches up quite well with this expectation.

Salt water

To effectively demonstrate the effect of active cooling through vacuum distillation, the experiment was set up in the same way as the other vacuum distillation run, except the feed reservoir in this run was artificially salted water instead of ultra pure water. For AGMD, the salted water produced a lower flux as a result of a steeper energy cost of distillation. Using this knowledge, flux for this experiment can be predicted to be around 1.38LMH, using equations 4.1 and 4.5 once again.

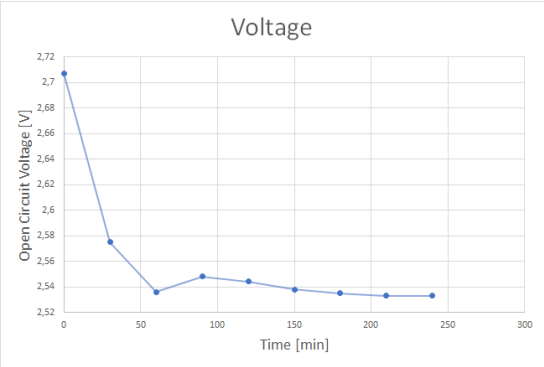

Figure 7.17. Open circuit voltage over the 4 hour run time

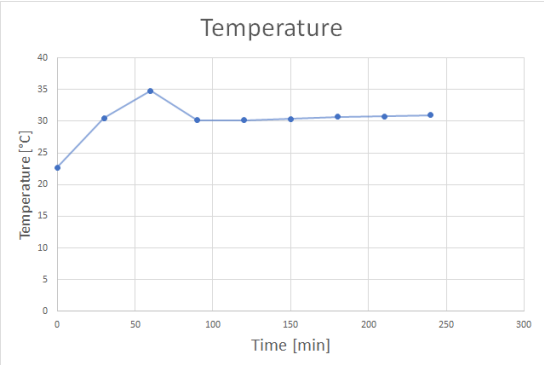

Figure 7.18. temperature behind the panel over the 4 hour run time

It is noteworthy that temperature so radically decreases after the pump was turned on, as this was not observed to a similar extent without salt present in the feed solution. Similarly, voltage spikes after the pump was turned on and the water cooling effectively became active. One potential explanation is that salt water has significantly higher enthalpy of vaporization, and so each molecule that turns from liquid to gas and diffuses across the membrane brings more energy with it. Whether this can explain such a large drop in temperature is worthy of investigation.

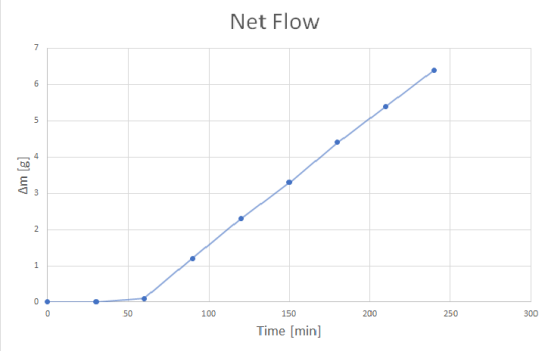

Figure 7.19. Net flow over the experiment

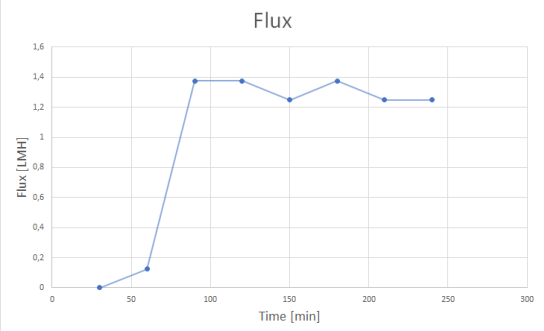

Figure 7.20. Calculated flux in LMH over the course of the experiment

Flux develops almost exactly as predicted by theory; around 1.38 LMH was predicted using the membrane coefficient obtained from the AGMD salt experiment, and the observed value is an average of 1.31 LMH.

7.2.4 Statistical analysis of early experiments

Seeing as five experiments have been presented, and further experiments are expected to produce significantly different results, it is apt to present a small statistical analysis of the previous experiments. As explained in section 5.3, the analysis was performed to gauge the standard deviation and present a more thorough comparison between experimental setups.

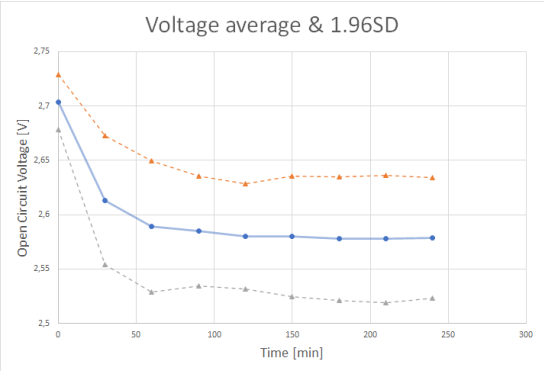

Figure 7.21. Voltage and upper and lower bounds for 95% confidence

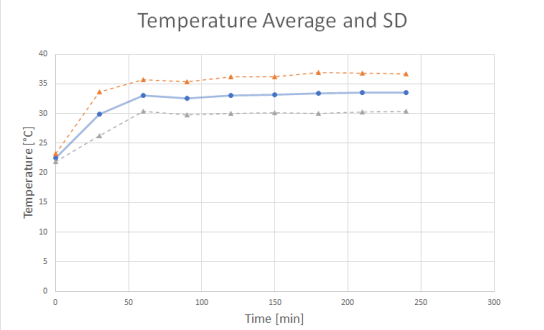

Figure 7.22. Temperature and upper and lower bounds for 95% confidence

Figures 7.21 and 7.22 show the average lines in full, as well as the upper and lower bounds for statistical significance in dotted lines. Future data points crossing these dotted lines will indicate a significant change in the results, allowing a slightly more robust assessment of the impact any system setup change may have.

7.2.5 Heated reservoir

To investigate impacts of continued operation at higher temperatures, to simulate a system where heat is overabundant, the setup was reconstructed to incorporate a circulatory peristaltic pump and a much larger reservoir to account for the added dead volume. The salted water in this reservoir was then heated to 60°C and run in a closed loop through the module.

AGMD at high temperature

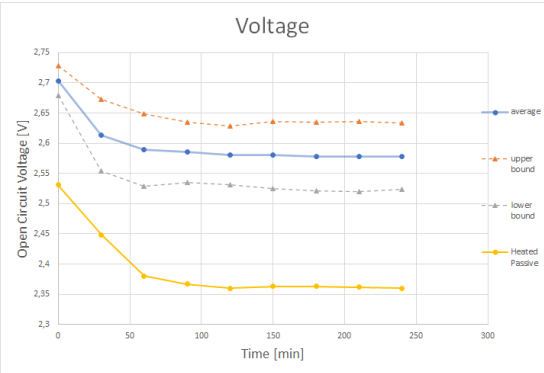

Figure 7.23. Open circuit voltage over the 4 hour run time

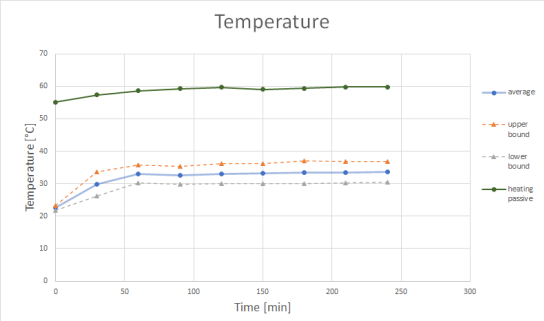

Figure 7.24. Temperature behind the panel over the 4 hour run time

Temperature develops much to the expectation of the setup; as it remains high throughout the experiment. The voltage seen in this experiment both starts and ends significantly lower than those found in other experiments, meaning far more heat was likely accumulated in the cells. This is because transport of heat is actively inhibited or even reversed as

the feed water is likely a very similar temperature to the cells themselves. Voltage is significantly lower than in the base set at every measurement.

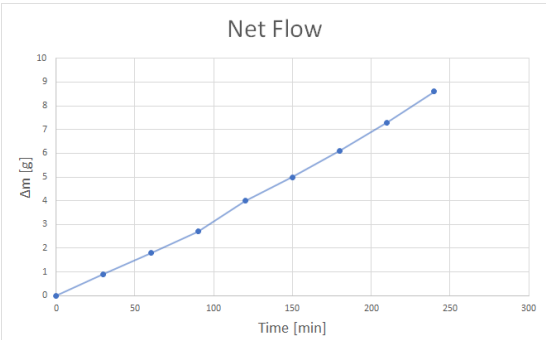

Figure 7.25. Net flow observed over the 4 hour run time

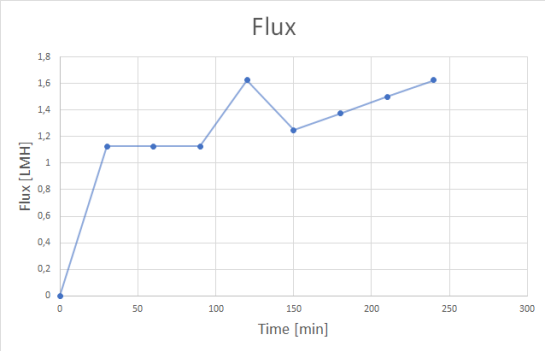

Figure 7.26. Flux calculated from flow over the course of the experiment

The flux initially seems surprising, as the prediction for a system of 60 degree saltwater feed and 22 degree pure water permeate would yield a flux of around 4.8 LMH with this membrane. This is far from what has been observed, however, but it highlights a very important phenomenon that has likely caused slight flux decreases in other experiments as well: the entire module heats up over the course of the experiment, leading to higher temperature and thus higher vapor pressure in the permeate chamber. Given a flux around 1.4LMH on average, the temperature in the permeate can be estimated to be 49.4 °C

Vacuum MD at high temperature

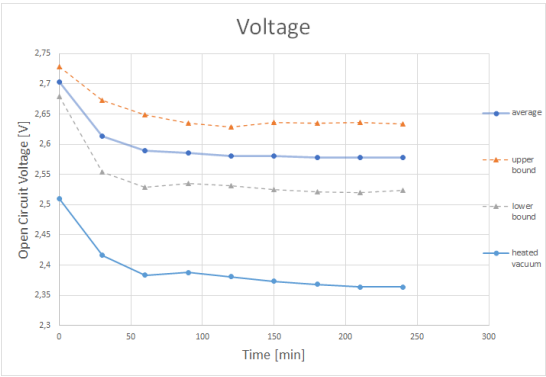

Figure 7.27. Open circuit voltage over the 4 hour run time

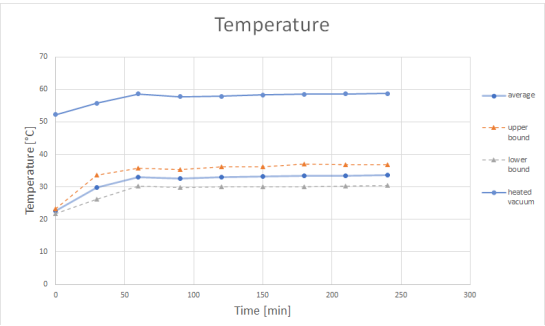

Figure 7.28. temperature behind the panel over the 4 hour run time

As in all previous VMD experiments, the pump was turned on after an hour of run time. This change in conditions has a small impact on both temperature and open circuit voltage, as the voltage increases a little between 60 and 90 minutes, and the opposite is true for temperature.

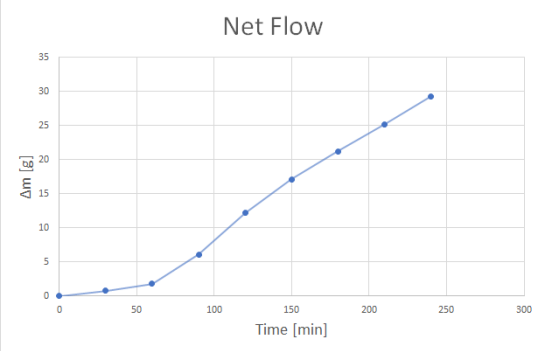

Figure 7.29. Net flow observed over the 4 hour run time

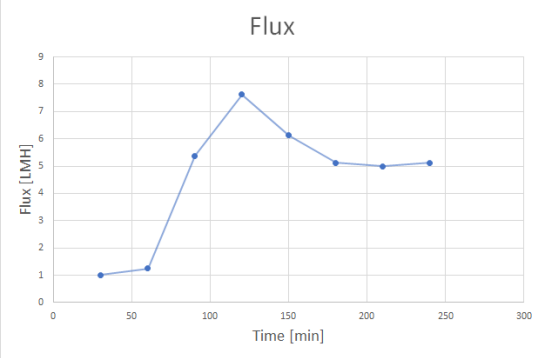

Figure 7.30. flux calculated from flow over the course of the experiment

The flux from this run peaks at a very high value before becoming stable around the expected value. around 5.5LMH was predicted, and after an initial peak, the system appears to enter some steady state with a flux around 5 LMH.

7.2.6 Heatsink experiments

It has been made clear that low PV-to-feed heat transfer rate has inhibited MD performance, and so a metallic heat sink was attached to the panel inside the feed chamber. Experiments were then performed in accordance with the established work-flow.

AGMD with heat sink installed

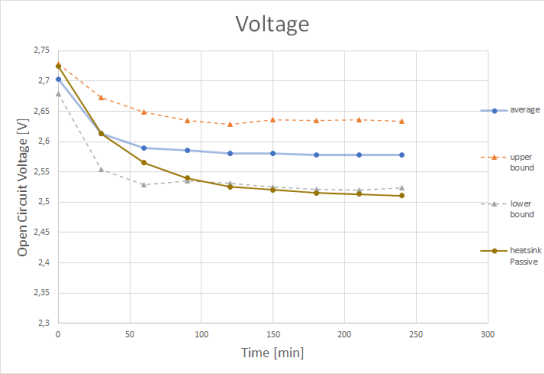

Figure 7.31. Open circuit voltage over the 4 hour run time

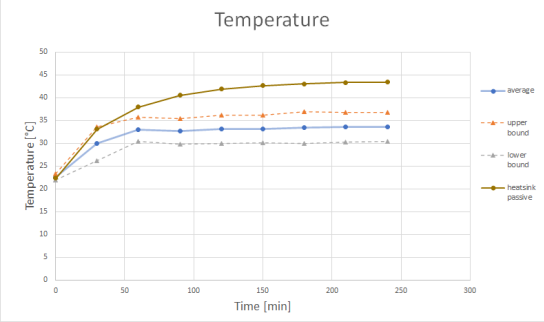

Figure 7.32. Temperature behind the panel over the 4 hour run time

It is quite clearly observed that temperature increases to significantly higher levels in this experiment when compared to the statistical average. The reason for this is likely a combination of the heatsink increasing the thermal energy transfer rate from PV to feed solution, and the simple fact that the heat sink displaces 5-6mL of the chamber's total volume, reducing the volume of water that is able to take the energy. Contrary to expectation, the latter half of this experiment shows a significantly lower open circuit voltage compared to earlier experiments.

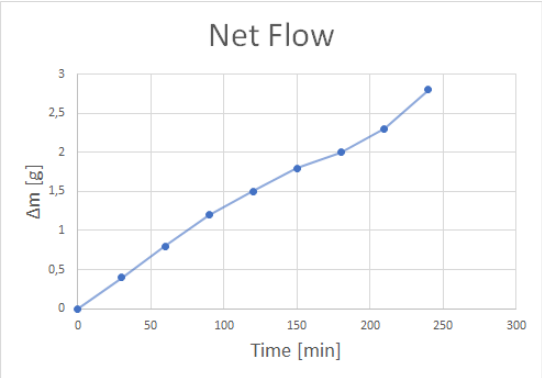

Figure 7.33. Net flow observed over the 4 hour run time

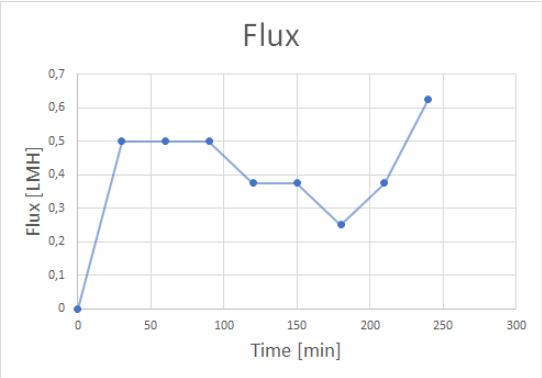

Figure 7.34. Flux calculated from flow over the course of the experiment

Given this flux graph, it is becoming increasingly apparent that AGMD in this configuration suffers from the permeate chamber heating up as time passes, as the expected flux given theory and an expectation of steady 22°C on the permeate side yields 2.15 LMH. Using equations 4.1 and 4.5 in reverse to calculate the permeate temperature given the actual observed flux yields a temperature of 39.5°C

Vacuum MD with heat sink installed

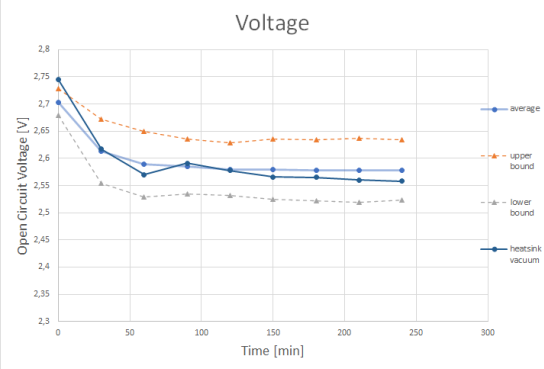

Figure 7.35. Open circuit voltage over the 4 hour run time

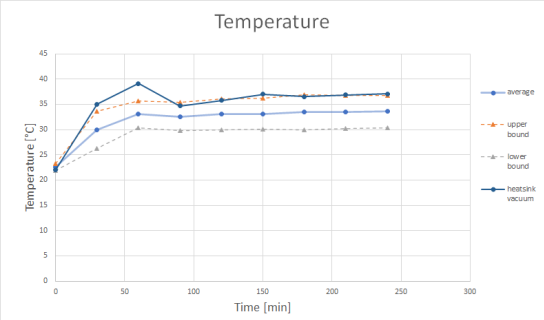

Figure 7.36. Temperature behind the panel over the 4 hour run time

This experiment responded quite intensely to the activation of the pump after the first hour of run time. This can be clearly observed from all graphs, as voltage increases, temperature decreases, and flux increases; all these responses are quite significant. Still, only the temperature displays a significant difference compared to early experiments. It is also noteworthy that the initial voltage data point is significantly higher than expected - one potential explanation for this is that higher heat transfer into the metal pieces is able to displace some of the initial heat that would otherwise be trapped in the cells, slowing down the heating process.

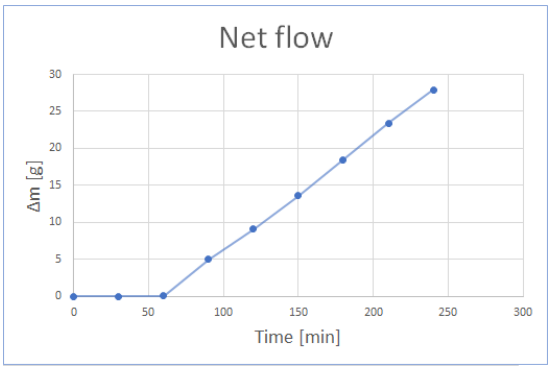

Figure 7.37. Net flow observed over the 4 hour run time

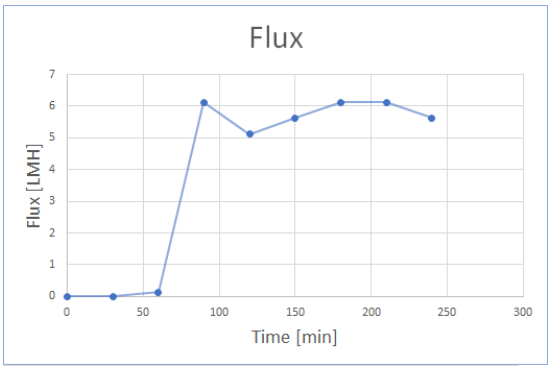

Figure 7.38. flux calculated from flow over the course of the experiment

Flux in this experiment remained far higher than predicted. The most likely reason behind is another transport mechanism was contributing, whether this means a small leak or the membrane wetting under continued pressure driven experiments is left ambiguous.

7.3 Ceramic membrane experiments

The unsuccessfully modified membrane piece was also tested as a more traditional cooling system, where water enters the membrane, absorbs heat from the panel, and permeates the membrane without significant distillation occurring. This is fundamentally a different process of energy transfer, as the mechanism is not latent heat transfer over the membrane, rather convection into the water and then mass transfer across the membrane. As such, the membrane functions less as a barrier, and more as transport inhibitor, reducing the flow rate of the open system. As such, the experiments should not be regarded as membrane distillation or evaporative cooling, rather traditional water cooling closer to what was done by Taqwa et al. [13]

7.3.1 Slow water flow cooling with ceramic membrane

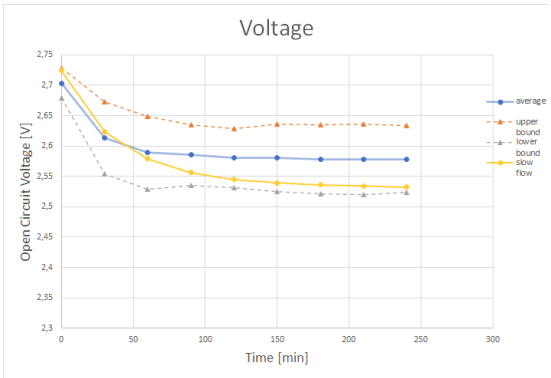

Figure 7.39. Open circuit voltage over the 4 hour run time

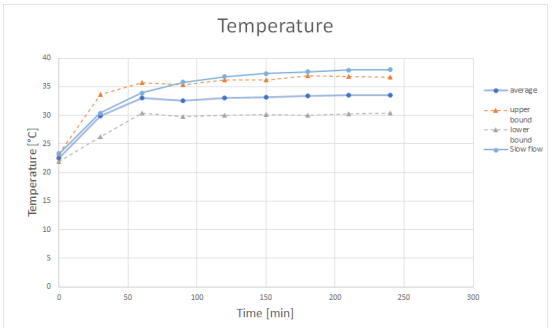

Figure 7.40. temperature behind the panel over the 4 hour run time

The slow flowing water heats up quite fast, and to significantly higher temperatures than the standard range as time passes. The voltage develops quite poorly, although barely not significantly worse than the standard range.

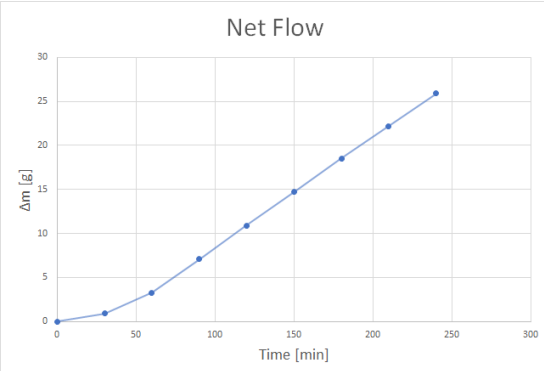

Figure 7.41. Net flow observed over the experimental runtime

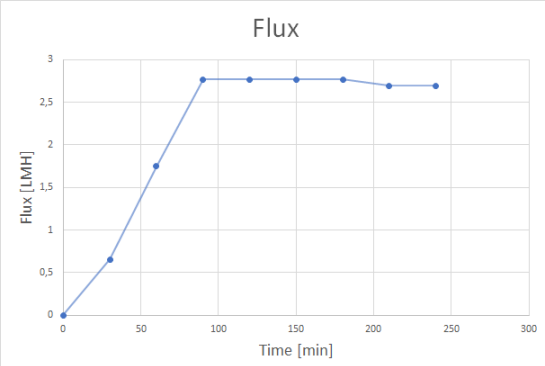

Figure 7.42. Flux calculated from flow during the experiment

The flux starts relatively slowly compared to its steady state value. Whether this is because faster flow occurs at higher temperatures or because there is some kinetic mechanism for the membrane to fully wet and become permeable would be hard to explain without further investigation.

7.3.2 Fast water flow cooling with ceramic membrane

The other piece of the membrane was also tested. This piece displayed a higher flow rate when wetted under the same conditions, and so it is interesting to see how this impacts the data produced.

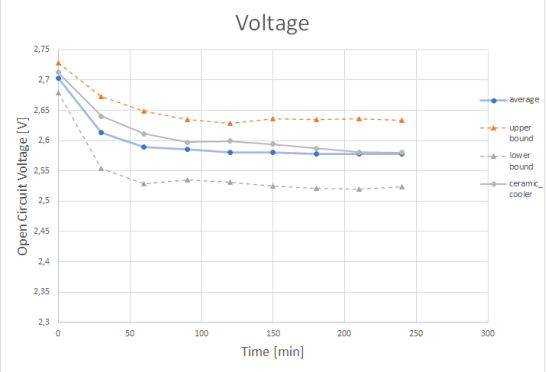

Figure 7.43. Open Circuit Voltage recorded over 4 hour run time

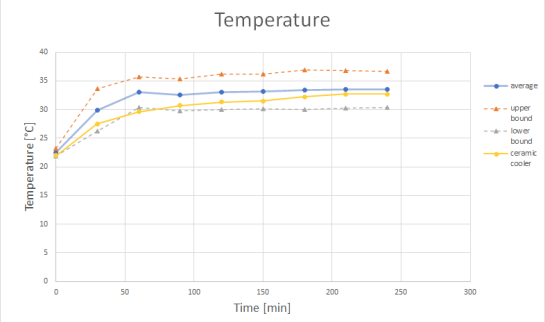

Figure 7.44. Temperature behind the panel over the recorded run time

It should be immediately noted that both voltage and temperature remain higher and lower than averages obtained previously, respectively. It should also be made clear that this observation is mostly outside of the significant range, apart from the slower temperature growth in the start of the experiment. If compared directly to the blank, the open circuit voltage remains slightly lower in this experiment, but this is again insignificant.

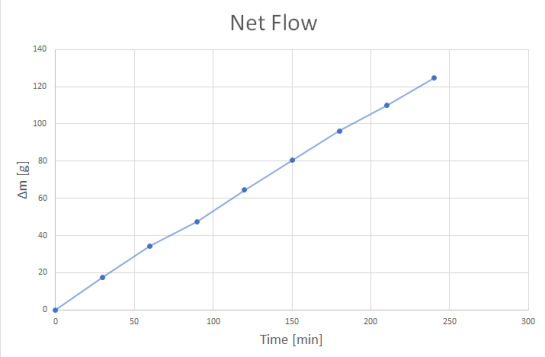

Figure 7.45. Net flow observed over experimental duration

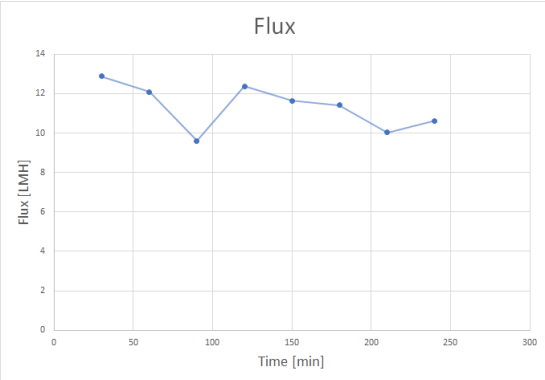

Figure 7.46. Flux calculated from flow observed during the experiment

While these values may seem exceedingly high at a glance, the mechanism of mass transfer is not distillation, and so a much higher flow was expected due to the membrane wetting and allowing heated saltwater to pass through immediately. The increases in flux can be ascribed to the reservoir being refilled at those intervals, and so pressure on the membrane was slightly higher.

7.4 Membrane coefficient calculations

While flux has been estimated under the assumption that temperature and membrane coefficient remain constant, it is also possible to perform the reverse calculation: flux and temperatures can be used to estimate C_m. This value is theoretically constant so long as the membrane functions, meaning any outliers or significant differences would indicate that the process is no longer running as intended. Therefore, a boxplot of each experiment utilizing the polymeric MD membrane is presented below:

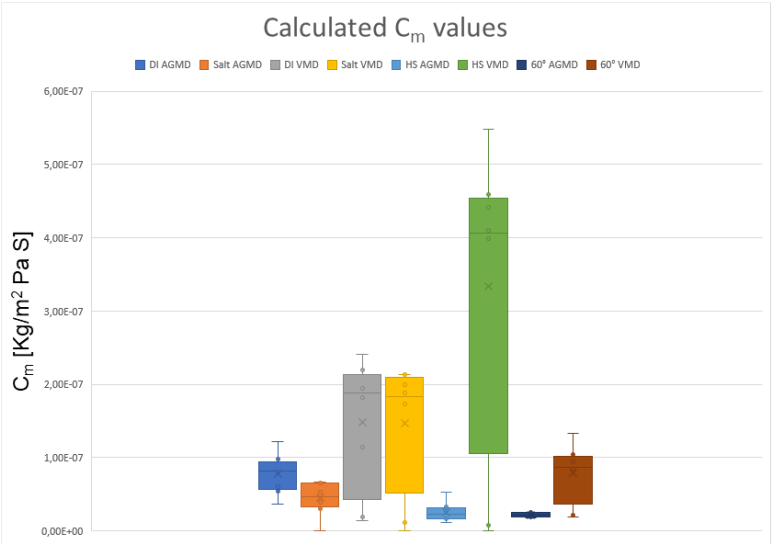

Figure 7.47. boxplot of all experiments with PTFE-based membrane

From figure 7.47 it becomes apparent yet again that certain experiments had issues.

The heatsink AGMD (abbreviated HS AGMD in the graph) for example has a very low calculated C_m due to the low flux. This low flux has previously been established as a product of P_p rising dramatically in the module, and this manifests in the C_m calculation. On the contrary, the heatsink VMD experiment (abbreviated HS VMD) shows the highest C_m, and this further supports that the transport mechanism is not exclusively through MD. Overall, the majority of experiments have their average C_m around $1-2*10^{-7}\frac{Kg}{m^2PaS}$. This number is somewhat low compared to what Hwang et al. found [43], however the paper correlates an increase in temperature polarization to a decrease in the theoretically calculated C_m value.

The ceramic experiments were not included into this graph because C_m is typically a value derived for MD specifically, and because no significant MD took place in these experiments, it would be wrong to include it as such.

7.5 Energy displacement and efficiency

During all experiments with the polymeric membrane present, water was displaced by evaporation across the membrane. Mechanically, this worked to expectation, and flux can be connected to an evaporative cooling effect due to the latent heat transfer. The amount of energy displaced from the feed solution by this mechanism can be calculated. Following a the formula seen below, the energy flux over the membrane can be calculated:

$$Q_h = \frac{\Delta m \cdot \Delta H_{vap}}{t_{exp}} \tag{7.2}$$

Where Δm is mass transfer over the course of the experiment, ΔH_{vap} is the latent heat of vaporization for the solution, and t_{exp} is the experimental run time. Performing this operation for all experiments yields a heat flux which can be compared between runs. It should be noted that the ceramic experiments are also included in this table, but the calculation is a numerical integral of the heat displaced as the water flowed instead the formula seen in equation 7.2.

Experiment	$Q_h[W]$
DI AGMD	0.70
Salt AGMD	0.49
Heatsink AGMD	0.50
Heated AGMD	1.55
DI VMD	1.8
salt VMD	1.15
heatsink VMD	5.01
heated VMD	5.27
Low flux ceramic	0.12
High flux ceramic	0.36

Table 7.1. Energy displacement in watts for each experiment

For all AGMD- and flow experiments it makes sense to calculate a theoretical efficiency given the irradiance from the sun simulator. The sun simulator was set to irradiate at $185\frac{mW}{cm^2}$, and the area of the irradiated surface was a circle with a 2.5cm radius. This

produces an irradiance of around 3.63 watts, and from there it is possible to define the energy displacement index (EDI) as $\frac{Q_h}{irradiance}$:

Experiment	*EDI*
DI AGMD	0.19
Salt AGMD	0.13
Heatsink AGMD	0.14
Low flux ceramic	0.03
High flux ceramic	0.10

Table 7.2. Energy displacement index for AGMD experiments

Experiments where the feed solution was heated by outside sources, as well as the VMD experiments were neglected on table 7.2 due to the fact that the energy source for the process was not exclusively the light from the source, meaning that the EDI would be incorrect. It would be possible to estimate a system EDI, if the energy required to run the pump and/or heater was also considered, but the pump used in this work consumes far more energy than required for such a small chamber, meaning that the result would be an extremely low and unrealistic EDI value.

7.6 Summation

So far data has been primarily presented in the form of graphs that showcase the development of a single experiment as its duration elapses. To better compare experiments between each other, a summary table is presented, where start and end temperatures, voltages, and flux as well as expected flux are presented. Data that performs significantly better than the average - meaning higher open circuit voltage or lower temperature - will be highlighted in green, and vice versa in red. Although there is no statistical analysis on flux, interesting values will also be highlighted

Experiment	T_0	T_{end}	V_0	V_{end}	J_{est}	J_{end}
Blank	22.1	35.1	2.725	2.603	N/A	N/A
DI AGMD	22.3	33.0	2.701	2.612	N/A	0.75
Salt AGMD	23.1	33.2	2.698	2.580	N/A	0.55
DI VMD	22.4	35.5	2.686	2.565	2.00	2.4
Salt VMD	22.7	31.0	2.707	2.533	1.38	1.31
Average	22.5 $\pm$0.68	33.56 $\pm$3.18	2.703 $\pm$0.025	2.577 $\pm$0.055	N/A	1.25
Heated AGMD	55.1	59.88	2.531	2.360	4.8	1.4
Heated VMD	52.3	58.7	2.510	2.364	5.5	5.8
Heatsink AGMD	22.3	43.4	2.725	2.511	2.15	0.45
Heatsink VMD	22.1	37.1	2.745	2.558	2.41	5.5
Low-flow Ceramic	23.3	38	2.724	2.532	N/A	2.63
High-flow Ceramic	22.0	32.7	2.713	2.58	N/A	10.4

Table 7.3. experimental data for all runs summarized

From this table it becomes much more apparent that increasing the temperature in the

feed chamber by increasing heat transfer does not immediately yield the expected increase in flux and evaporative cooling. The reason for this has been explained above: the entire module heats up over time, and as there is no effective transport mechanism for heat away from the permeate chamber, $[p_f - p_p]$ remains small. This could be alleviated by running multiple membrane processes in a stack, so that p_1 will supply heat to an f_2 stream. [41, 44] For the ceramic part, it seems clear that the faster flow rate outperforms, as voltage is slightly higher, and temperature remains relatively more stable throughout the run.

8 Discussion

8.1 PV characterization

The PV used in this work had 12 cells of dimensions 1.8x2.5cm, and the IV diagram revealed a short circuit current of 200mA, while the maximum open circuit voltage was found to be around 3.3V. The fill factor was demonstrated in figure 7.2 to be about 0.61, enabling the characterization of the panel's expected PCE to be 6.2 under radiation density of 1200 $\frac{W}{m^2}$. It is expected that the panel would have a relatively low PCE compared to the market standard, so this value seems quite realistic. It is important to understand that if this value were higher it would likely influence the EDI calculated in later sections, as more electricity production necessitates less heat production given the same irradiance, although quantifying this difference in EDI is a dubious task without a similar study on a superior PV.

8.2 Synergistic water production via Polymeric AGMD and VMD

It has been shown in previous studies that a PV-MD combined module is feasible, and that synergistic electricity and water production may even enable a higher efficiency for the PV. [41, 44] This work has demonstrated that the contrary is also achievable, as open circuit voltage was shown to be significantly reduced in some experiments at steady state. This is established as due to the lack of mass - and therefore also heat - transport away from the feed chamber of the MD module, which inhibited waste heat escaping the PV, reducing PCE, specifically open circuit voltage.[40] This paired with significantly higher temperature readings in those same experiments demonstrates the link between these values, and shows some of the dichotomy that this technological combination can have. Alleviating this issue has been shown to be possible by the aforementioned studies, as they achieved success by running multiple membrane modules in a stack, so as to supply an escape route for the heat once it reaches the permeate chambers. The alternative solution to this issue is to run VMD instead of AGMD, as it reduces the impact of permeate temperatures, since the vapor pressure is forced very low.[8] This work focuses on this, as VMD was employed in an attempt to assess the impact on the evaporative cooling effect, as well as its impact on pure water production. PV-VMD in this work is almost consistently shown to function according to the known theory of MD and the well established Clausius-Clapeyron equation.[8] In at least one example, the VMD setup attained a higher steady state temperature than its AGMD counterpart, suggesting that VMD has some advantage in terms of heat transfer from panel to feed stream. A possible explanation is that a small

layer of air forms between the panel and the water in the feed chamber under AGMD conditions; the vacuum applied to the permeate side would then potentially suck this air through, filling the feed chamber up completely and improving heat transfer. Additionally, theoretical C_m values were calculated for all experiments and shown in a box plot on figure 7.47. The calculated C_m values are somewhat low compared to literature [43], and the likely reason for this is the effect of temperature polarization, as there is essentially no flow velocity in the feed for most experiments. This lack of flow likely led to large boundary layers, and thus a high temperature polarization, which meant bulk temperature readings, and by extension the calculated C_m, were more incorrect than if a cross flow had been implemented. EDI values were calculated using the heat enthalpy of vaporization and the weight loss from the reservoir to estimate the amount of energy that was captured and employed for MD. This was only done for AGMD experiments, however, as the energy required to run the pump was magnitudes higher than what would have been necessary, and so EDI values for VMD experiments would have been misleading - either too high if the pump's energy intake was neglected, or too low if it was considered.

8.3 Ceramic membrane experiments

The ceramic membrane was modified with methylated silica particles, calcinated, and later dip coated in methylated silica particles to grant hydrophobicity. The aim was originally to produce a surface hydrophobic enough to retain the salt water and perform MD as was done with the PTFE membrane. A similar modification has been seen in Si-C membranes in the past, using an F-POSS approach. [28] The modification in this work was unsuccessful, as both pieces - originally cut from the same tube of Si-C membrane - were shown to be wettable, but their permeation rate was different. As such, the investigation of flow rate impact on system performance was launched, and it seems relatively clear that the higher flow rate performed better in terms of temperature, as it increased slower and to a much lower value over the duration. Voltage was also slightly better in this experiment, although neither experiment had a significant impact on open circuit voltage overall. This demonstrates an important realization, however: it is possible to separate the processes and achieve similar PV performance. Indirect PV-MD utilization brings a lot of interesting challenges and opportunities, such as decoupling the ratio of membrane area to cell area, and cost optimizing operating temperature of MD to increase performance. With the use of efficient heat exchange mechanisms, this decoupling could enable MD to run at high temperatures, while a high flow rate at the panel enables effective cooling. At scale, this would allow for effective harvest of the vast amounts of low-grade thermal energy available in PV farms, while either not impairing their operation or even improving PCE if built correctly. It should be noted in this discussion point, however, that higher flow rate in this system means the permeating salt water stream will be heated less than if the flow rate were lower, making the concentration of heat more troublesome.

9 Conclusion

In this work, a strategy for a combined PV-MD module using a single polymeric membrane was realized. At the same time, a modified Si-C membrane module was also constructed to produce a steady flow of salted water to cool the panel. While MD was successfully maintained for 4 hours under multiple configurations using the former, it did not positively impact the open circuit voltage of PV as initially expected. The reason for this is that the system lacked an effective mechanism of dissipating the heat once it has been utilized for MD. This lead to the membrane system effectively "stalling" which delayed further transfer of heat and mass, and a further build-up of heat in the PV. Still, the single membrane outperforms its ceramic counterpart in terms of energy displacement, seemingly utilizing more heat from the PV. The system stalling was also shown to be avoidable when employing VMD as opposed to AGMD, as can be seen from the heated VMD producing significantly more pure water than its AGMD counterpart. The ceramic solution also had some considerable benefits: most notably the open circuit voltage was less diminished than certain PV-MD experiments. In terms of the flow method for dissipating heat, the faster flow rate outperformed its counterpart both in terms of the open circuit voltage and EDI. The faster flow rate enabled a better heat transfer, as the passing water was on average colder than if the flow rate was lower. Using a pressure driven heat exchange mechanism, the heat of this stream could be concentrated to temperatures more suitable for MD. This would in principle lead to an effective decoupling of the technologies, while maintaining the benefits that they can demonstrably provide each other. Overall, the problems of heat transfer mechanisms plague the effect on PV efficiency, as multiple experiments significantly reduce the open circuit voltage. This work has demonstrated the necessity of either stacking multiple membrane chambers as seen in other works [41, 44], or running the system as VMD to maintain higher mass- and heat transfer if effective direct PV-MD coupling is to be achieved.

10 Further work and Perspective

This work presents a number of interesting findings, namely a reason for the use of multiple membranes in other PV-MD systems, a method for running PV-VMD somewhat successfully with a single membrane, and the potential for a water cooling system wherein the MD process may occur separately. A number of topics are either opened up and not fully explored, or due to some constraints on time and equipment, more experiments could have been conducted to further enhance the understanding.

- In the work, a small statistical analysis was performed on the first 5 experiments, to provide a method of comparison to all latter experiments. Repeating those 5 experiments, or even a smaller set of experiments with a larger data sample would have allowed to better detect differences, or a higher statistical power.
- The beam size of the lamp used in this work was rather small, and set to a very high intensity to ensure the production of useful data despite the small working area. It would have been insightful to conduct experiments on a larger scale and in an outdoor environment, to better understand and work around the challenges such an environment would produce.
- The last set of results presented are related to a different process than MD's evaporative cooling effect, and it is stated that this flow-based cooling system would be effective in combination with a pressure driven heat exchange mechanism to concentrate the thermal energy. This was not explored as of this work, however, and should be considered a challenge for future studies in the field of PV enhancement and waste heat utilization.

Bibliography

[1] H. A. Hassan and A. A. Rasheedy., "The Nile River and Egyptian foreign policy interests ," *African sociological Review*, pp. 25–37, 2007.

[2] S. G. Setegn, D. Rayner, A. M. Melesse, B. Dargahi, and R. Srinivasan, "Impact of climate change on the hydroclimatology of Lake Tana Basin, Ethopia," *Water Resources Research*, 2011.

[3] H. Chen and A. Swain, "The Grand Ethiopian Renaissance Dam: Evaluating Its Sustainability Standard and Geopolitical Significance," *Energy Development Frontier*, pp. 11–19, 2014.

[4] A. Sherwani and V. J.A. Usmani, "Life cycle assessment of solar pv based electricity generation systems: A review," *Renewable and Sustainable Energy Reviews*, vol. Journal 14/2010, pp. s. 540–544, 2010.

[5] B.Tremeac and F. Meunier, "Life cycle analysis of 4.5mw and 250w wind turbines," *Renewable and Sustainable Energy Reviews*, vol. Journal 13/2009, pp. s. 2104–2110, 2009.

[6] K. Smolders and C. Franken, "Terminology for Membrane Distillation," *Desalination*, pp. 249–263, 1989.

[7] H. M. Cassard and H. G. Park, "How to select the optimal membrane distillation system for industrial applications," *Journal of Membrane Science*, vol. 56, pp. 978–982, nov 2018.

[8] A. Alkhudhiri, N. Darwish, and N. Hilal, "Membrane distillation: A comprehensive review," *Desalination*, vol. Journal 287/2012, pp. s. 2–18, 2012.

[9] *Fundamentals of Materials for Energy and Environmental Sustainability*. CAMBRIDGE, 2011.

[10] P. K. Nayak, S. Mahesh, H. J. Snaith, and D. Cahen, "Photovoltaic solar cell technologies: analysing the state of the art," *Nature Reviews Materials*, vol. 4, pp. 269–285, mar 2019.

[11] C. M.D.S.D, A. M.L.C, and W. H., "Temperature effect on solar photovoltaic power generation," *research gate*, p. 7, jan 2017.

[12] V. J. Fesharaki, M. Dehghani, and J. J. Fesharaki, "The effect of temperature on photovoltaic cell efficiency," *t International Conference on Emerging Trends in Energy Conservation - ETEC*, p. 6, nov 2011.

[13] A. Taqwa, T. Dewi, R. Kusumanto, C. R. Sitompul, and Rusdianasari, "Automatic cooling of a PV system to overcome overheated PV surface in palembang," *Journal of Physics: Conference Series*, vol. 1500, p. 012013, apr 2020.

[14] S. Bewick, R. Parsons, T. Forsythe, S. Robinson, and J. Dupon., "Phase diagram for water." `https://chem.libretexts.org/Bookshelves/Introductory_Chemistry/Book%3A_Introductory_Chemistry_(CK-12)/13%3A_States_of_Matter/13.20%3A_Phase_Diagram_for_Water`, Jul 2021.

[15] R. Schofield, A. Fane, and C. Fell, "HEAT AND MASS TRANSFER IN MEMBRANE DISTILLATION," *Journal of Membrane Science*, pp. 299–313, 1987.

[16] M. Khayet, A. Velázquez, and J. I. Mengual, "Modelling mass transport through a porous partition: Effect of pore size distribution," *Journal of Non-Equilibrium Thermodynamics*, vol. 29, pp. 978–982, jan 2004.

[17] M. Khayet, T. Matsuura, J.I.Mengual, and M. Qtaishat, "Design of novel direct contact membrane distillation membranes," *Desalination*, vol. 192, pp. 105–111, May 2006.

[18] R. Schofield, A. Fane, and C. Fell, "Heat and mass transfer in membrane distillation," *Journal of Membrane Science*, vol. 33, no. 3, pp. 299–313, 1987.

[19] J. Phattaranawik and R. Jiraratananon, "Direct contact membrane distillation: effect of mass transfer on heat transfer," *Journal of Membrane Science*, vol. 188, no. 1, pp. 137–143, 2001.

[20] M. Qtaishat, T. Matsuura, B. Kruczek, and M. Khayet, "Heat and mass transfer analysis in direct contact membrane distillation," *Desalination*, vol. 219, no. 1, pp. 272–292, 2008.

[21] P. Termpiyakul, R. Jiraratananon, and S. Srisurichan, "Heat and mass transfer characteristics of a direct contact membrane distillation process for desalination," *Desalination*, vol. 177, pp. 133–141, jun 2005.

[22] H. Fogler, *Elements of chemical reaction engineering.* Harlow, Essex: Pearson, 2014.

[23] K. W. Lawson and D. R. Lloyd, "Membrane distillation," *Journal of Membrane Science*, vol. 124, pp. 1–25, feb 1997.

[24] S. Gersten, *Physics and Chemistry of Mater.* John Wiley and Sons, 2001.

[25] R. N. Wenzel, "Resistance of solid surfaces to wetting by water," *Industrial and Engineering Chemistry*, vol. 28, pp. 988–994, aug 1936.

[26] A. Franken, J. Nolten, M. Mulder, D. Bargeman, and C. Smolders, "Wetting criteria for the applicability of membrane distillation," *Journal of Membrane Science*, vol. 33, no. 3, pp. 315–328, 1987.

[27] S. Krajewski, W. Kujawski, M. Bukowska, C. Picard, and A. Larbot, "Application of fluoroalkylsilanes (FAS) grafted ceramic membranes in membrane distillation process of NaCl solutions," *Journal of Membrane Science*, vol. 281, pp. 253–259, sep 2006.

[28] V. Boffa, C. Lunghi, C. A. Quist-Jensen, G. Magnacca, and P. Calza, "Fabrication and surface interactions of super-hydrophobic silicon carbide for membrane distillation," *Nanomaterials*, vol. 9, p. 1159, aug 2019.

[29] C. Brinker, *Sol-gel science : the physics and chemistry of sol-gel processing.* Boston: Academic Press, 1990.

[30] S. K. Hubadillah, Z. S. Tai, M. H. D. Othman, Z. Harun, M. R. Jamalludin, M. A. Rahman, J. Jaafar, and A. F. Ismail, "Hydrophobic ceramic membrane for membrane distillation: A mini review on preparation, characterization, and applications," *Separation and Purification Technology*, vol. 217, pp. 71–84, jun 2019.

[31] H. Yang, P. Pi, Z.-Q. Cai, X. Wen, X. Wang, J. Cheng, and Z. ru Yang, "Facile preparation of super-hydrophobic and super-oleophilic silica film on stainless steel mesh via sol–gel process," *Applied Surface Science*, vol. 256, pp. 4095–4102, apr 2010.

[32] C. Neinhuis and W. Barthlott, "Characterization and distribution of water-repellent, self-cleaning plant surfaces," *Annals of Botany*, vol. 79, pp. 667–677, Jan. 1997.

[33] D. U. S. D. Laboratory, 9 2020. `https://www.sdlab-dankook.com/research-1`.

[34] J. Fierro, ed., *Metal Oxides: Chemistry and Applications.* No. 108 in Chemical Industries, e: Taylor & Francis Ltd., 1 ed., 2005.

[35] A. L. Stanford and J. M. Tanner, *Physics for Students of Science and Engineering.* Burlington: Academic Press, Inc, 1985.

[36] D. A.Neaman, *Semiconductor Physics and Devices Basic Principles.* New York: Raghu Srinivasan, fourth ed., 2012.

[37] A. Belghachi, "Theoretical calculation of the efficiency limit for solar cells," *Physical Review*, vol. 56, pp. 978–982, oct 2015.

[38] K. Zweibel, *Basic photovoltaic principles and methods.* New York: Van Nostrand Reinhold, 1984.

[39] I. S. Maksymov, I. Staude, A. E. Miroshnichenko, and Y. S. Kivshar, "Optical yagi-uda nanoantennas," *Nanophotonics*, vol. 1, pp. 65–81, jun 2012.

[40] Y. Adel, R. Abdelhady, and A. Ibrahim, "Assessment of a proposed hybrid photovoltaic array maximum power point tracking method," *Water Science*, vol. 30, 12 2016.

[41] G. Antonetto, M. Morciano, M. Alberghini, G. Malgaroli, A. Ciocia, L. Bergamasco, F. Spertino, and M. Fasano, "Synergistic freshwater and electricity production using passive membrane distillation and waste heat recovered from camouflaged photovoltaic modules," *Journal of Cleaner Production*, vol. 318, p. 128464, 2021.

[42] M. H. Nielsen, "Silicon carbide membrane percrystallization by methylated silica modification.." Master thesis, Aalborg University, 2022.

[43] H. J. Hwang, K. He, S. Gray, J. Zhang, and I. S. Moon, "Direct contact membrane distillation (DCMD): Experimental study on the commercial PTFE membrane and modeling," *Journal of Membrane Science*, vol. 371, pp. 90–98, apr 2011.

[44] L. Huang, Y. Wang, R. He, X. Kong, S. Lei, Y. Liu, B. Wang, H. Jiang, H. Liu, K. Liu, and X. Hu, "Solar-driven co-generation of electricity and water by evaporation cooling," *Desalination*, vol. 488, p. 114533, aug 2020.